République Algérienne démocratique et populaire

Ministère de l'éducation supérieur et de la recherche scientifique

المدرسة الوطنية المتعددة التقنيات
Ecole Nationale Polytechnique

End-of-studies project
To obtain the mechanical engineering degree, entitled:

Numerical modeling of drilling fluid 'temperature during the transient state

Faid Mohamed Chaouki

Under the direction of   Mr. Said   Rechak   Professor at ENPA

Mr. Abdelouaheb   BOUGHELOUM   Engineer at SONATRACH

Presented and publicly defended on 19 September 2021

Composition of the jury

President	Mr. Arezki Smaili	Professor	ENP
Promoter	Mr. Said Rechak	Professor	ENP
Co-promoter	Mr. Abdeleouaheb Bougheloum	Drilling engineer	SONATRACH
Examiner	Mr. Mohammed Benbraika	Professor	ENP

ENP 2021

المدرسـة الوطنيـة المتعددة التقنيـات
Ecole Nationale Polytechnique

End-of-studies project
to obtain the mechanical engineering degree, entitled:

Numerical modeling of drilling fluid 'temperature during the transient state

Faid Mohamed Chaouki

Under the direction of   Mr. Said   Rechak   Professor at ENPA

Mr. Abdelouaheb   BOUGHELOUM   Engineer at SONATRACH

Presented and publicly defended on 19 September 2021

Composition of the jury

President	Mr. Arezki Smaili	Professor	ENP
Promoter	Mr. Said Rechak	Professor	ENP
Co-promoter	Mr. Abdeleouaheb Bougheloum	Drilling engineer	SONATRACH
Examiner	Mr. Mohammed Benbraika	Professor	ENP

ENP 2021

République Algérienne démocratique et populaire

Ministère de l'éducation supérieur et de la recherche scientifique

المدرسة الوطنية المتعددة التقنيات
Ecole Nationale Polytechnique

Projet de fin d'étude

Afin d'obtenir le diplôme d'ingénieur en mécanique, intitulé :

Modélisation numérique de la température du fluide de forage durant le régime transitoire

Faid Mohamed Chaouki

| Encadré par | Mr. Said | Rechak | Professeur à ENP |
| | Mr. Abdelouaheb | BOUGHELOUM | Ingenieur a SONATRACH |

Soutenu le 19 septembre 2021

Composition du jury

President	Mr. Arezki Smaili	Professeur	ENP
Promoteur	Mr. Said Rechak	Professeur	ENP
Co-promoteur	Mr. Abdeleouaheb Bougheloum	Ingénieur de forage	SONATRACH
Examinateur	Mr. Mohammed Benbraika	Professeur	ENP

ENP 2021

ملخص

نظرا لصعوبة استخراج المعطيات الحقيقية لسائل الحفر اثناء حفر الآبار المستخدمة لاستخراج المحروقات ، يتم الإعتماد على نماذج تساعد المهندسين على التنبؤ بدرجة حرارة سائل الحفر داخل البئر .

في هذا العمل، سيتم تقديم نموذج لتوزيع درجة حرارة سائل الحفر من خلال معرفة مختلف مصادر الطاقة التي يتعرض لها مع الاخد بعين الاعتبار تأثير كل من درجة الحرارة و الضغط على خصائص السائل مثل اللزوجة و الكتلة الحجمية و التي تؤثر بدورها على توزيع الحرارة.

النموذج المقدم في هذه المذكرة هو نموذج يدرس السائل في **حالته الإنتقالية** و هي دراسة شاملة تمكننا من تحديد حرارة السائل عند كل عمق و في اوقات مختلفة و حتى في حالته الثابتة . يتم اشتقاق النموذج عبر معرفة عبارات مختلف مصادر الطاقة و استعمال القانون الأول للديناميكة الحرارية التي تعطي معادلات تفاضلية يتم حلها بإستخدام طريقة الفوارق المنتهية.

Résume

Ce travail vise à étudier la distribution de la température du fluide de forage à l'intérieur d'un puits de forage. Le modèle de température est dérivé d'abord en énonçant les différentes sources d'énergie agissant sur le fluide. En les introduisant dans la première loi de la thermodynamique on retrouve un ensemble d'équations différentielles. Ces équations sont résolues en utilisant la méthode explicite des différences finies. Pour un modèle plus réaliste, l'effet de la pression et de la température sur les propriétés de la boue est pris en considération. Le modèle étudie le fluide pendant son état transitoire, nous permettant ainsi de prédire la température à chaque profondeur, et à tout moment de l'opération de forage. Les résultats sont comparés aux résultats existants dans la littérature et sont en bonne concordance.

Mots clés : Fluide, forage, transfert de chaleur, propriétés thermophysiques, température, pipe, annulus.

Abstract

This work studies the temperature distribution of drilling fluid inside a wellbore. The model of temperature is derived first by stating different energy sources acting on the fluid and then introducing them into the first law of thermodynamic leading to a set of differential equations. These equations are resolved using the explicit finite difference method. For a more realistic model, the effect of pressure and temperature on mud's properties is taken into consideration. The model studies the fluid during its

transient state, allowing us finally to predict the temperature at each depth, and any time of the drilling operation. The results are compared to the existing results in the literature and are in good agreements.

Key words: Fluid, drilling, heat transfer, thermophysical properties, temperature, pipe, annulus.

Acknowledgement

Dedications

I dedicate this modest work

To my parents and my sister, who are the most important people in my life and to whom I am so grateful and wish god keeps them safe for me.

To all my friends. Wish you more success in your lives.

Table of Contents

List of figures

List of tables

Nomenclature

$\dot{m}$ Mass flow (Kg/s)

C_p Specific heat rate ($/kg°C$)

k Thermal conductivity ($W/m.°C$)

ρ Density (kg/m^3)

v Velocity (m/s)

μ Viscosity ($Pa.s$)

h Convective heat transfer coefficient($W/m^2.C$)

Q Flow rate (m^3/s)

q'' Heat flux (W/m^2)

r Radius (m)

d Diameter (m)

T Temperature ($°C$)

U Overall heat transfer coefficient ($W/m^2.C$)

α Formation heat diffusivity (m^2/s)

P   pressure(Pa)

G Geothermal gradient (°C/m)

x Measured depth (m)

t Circulation time s

ϕ Energy source term (J/s)

dx Box length (m)

dr Radial step (m)

dt Step time (s)

Q Heat exchange (W)

E   Thermal energy (W)

n Number of boxes -

F   Axial force (N)

L   Length (m)

N_r Rotary pipe speed (1/min)

RPS Rotations per second (1/s) w Unit pipe weight N/m

μ Friction factor -

τ_q Torque N.m

Subscripts

a	Annulus
p	Pipe
w	Wellbore
f	Formation
i	Inner
o	Outer
c	Casing
D	Dimensionles

Chapter 01: Introduction, Literature review and problematic.

1.1 Introduction

To drill a well it is necessary to carry out simultaneously the following actions (drilling process):

- to overcome the resistance of the rock, crushing it into small particles measuring just a few mm;
- to remove the rock particles, while still acting on fresh material;
- to maintain the stability of the walls of the hole;
- to prevent the fluids contained in the drilled (Water) formations from entering the well.

This can be achieved by using rotary drilling rigs which are the ones operating today in the field of hydrocarbons exploration and production. The drilling rigs are complexes of mobile equipment which can be moved (onshore and offshore) from one drill site to another, drilling a series of wells. In rotary drilling the rock is bored using a cutting tool called the bit, which is rotated and simultaneously forced against the rock at the bottom of the hole by a drill string consisting of hollow steel pipes of circular section screwed together.
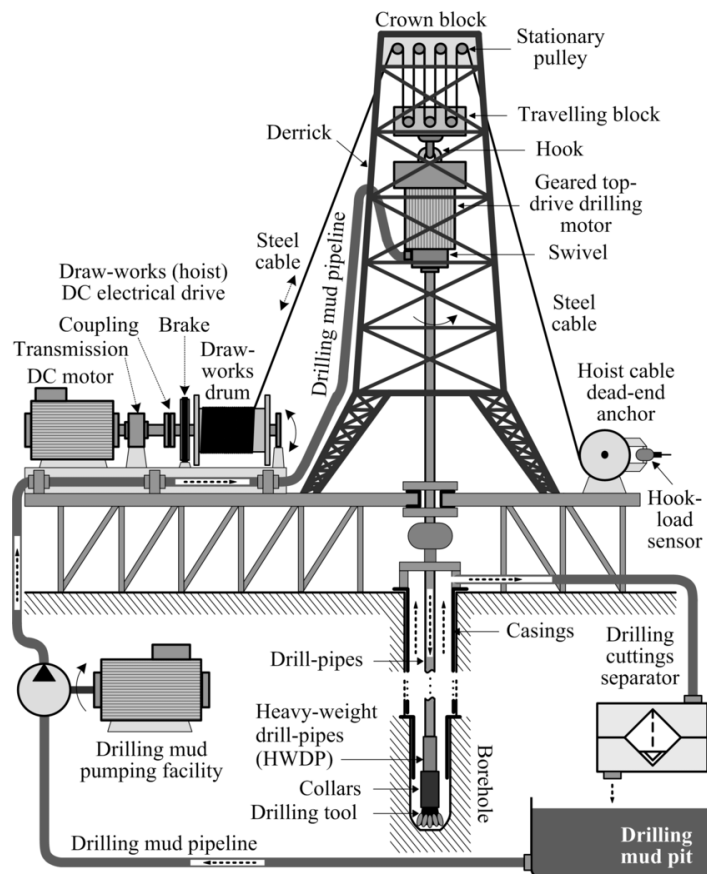
Figure 1. The drilling system

The cuttings produced by the bit are transported up to the surface by a drilling fluid, usually a liquid (mud or water), or else a gas or foam, circulated in the pipes down to the bit and back up the annular space between drill pipe and rock. Drilling fluid has several functions such as cleaning the bit, balancing in-situ pore pressure and even lubricating the drill string. The rotation is transmitted to the bit from the surface by a device called the rotary table or, in the modern rigs, by a top drive motor with the rotary table as backup; additional rotation can be added by downhole motors located directly above the bit. After having drilled a certain length of hole, in order to guarantee its stability, it has to be cased with steel pipes, called casings, joined together by threaded sleeves. The space between the casing and the hole is then filled with cement slurry to ensure a hydraulic and mechanical seal. The final depth of the well is accomplished by drilling holes of decreasing diameter, successively protected by casings, likewise of decreasing diameter, producing a structure made up of concentric tubular elements.[18]

With the trend toward deeper and consequently hotter holes, an accurate determination of the temperature distribution in circulating wells is important, and this is for a number of reasons.

Primarily, in order to achieve desired drilling fluid rheology, one requires accurate information of the temperatures experienced in the annulus. Knowledge of the radial thermal profile is also essential to determine the expansion of the casing annulus fluid and hence resulting stresses on the formation and prevent its fracture. Another requirement is during the cementing process where it is necessary to achieve turbulent cement flow to ensure maximum adhesion to the annulus walls. This flow pattern will depend on the viscosity of the cement, which is strongly influenced by the borehole temperature. Finally, in order to gain the U.K Health and Safety Executive (previously Dept of Energy) approval to drill An HPHT well in the UK sector of the North Sea (for instance), estimates of the mud return temperature at the BOP stack and topsides must be determined and shown to be below specified safety limits. [19]

Consequently, a better understanding of factors that affect temperatures during circulation and trips could improve drilling operations. It was toward the goal to obtaining this understanding that this study was directed.

To better understand the phenomena mentioned in the next chapters, a detailed description of the well is necessary.
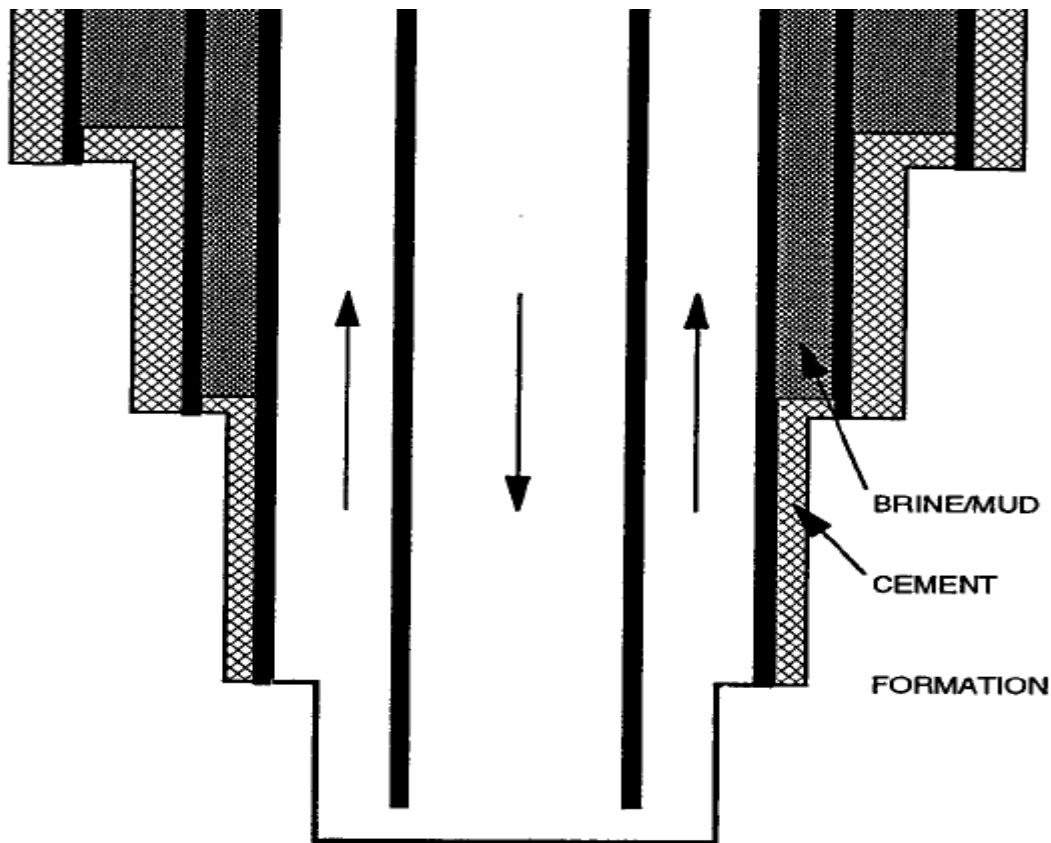
Figure 2. *Description of the well*

The figure above shows the 4-vertical layer, composing the well. Each layer has a different radial composition depending on the depth. The number of casings decreases while going deeper, so does the diameter of the hole. For each vertical layer, the Heat Transfer Coefficient of the part of the well in contact with the formation (the rock) changes which influences the temperature.

1.2. Literature review

Wellbore temperature modeling is still a challenge facing the drilling industry. Through the past decades, extensive efforts have been made towards accurate and precise modeling of the wellbore temperature while drilling. Modeling of the heat transfer inside the wellbore goes back to the early 1960s. The studies that have been conducted by **Edwardson et al. (1962), Ramsey (1962), Tragesser et al. (1967)** and **Raymond (1969)** are considered the base foundation for many later studies and models of wellbore temperature.

Holmes and Swift (1970) developed an analytical model to predict the fluid temperature in the drill pipe and the annulus while drilling with respect to depth.

Keller et al. (1973) proposed a model describing the two-dimensional heat transfer phenomenon in and around a wellbore. **Marshall and Bentsen (1982)** developed a computer-based model to determine the wellbore and the formation temperatures during transient state.

18

Hasan and Kabir (2012) discussed a general wellbore thermal model that can be applied to various situations. They verified their model using field case studies.

1.3. Problematic

The problematic is to determine the variations of drilling fluid's temperature, inside the pipe and the annulus section at different depths, during a transient state, where the temperature varies with time depending on the initial conditions of the fluid and its instantaneous conditions. The work presented here consists on finding a mathematical model based on physical assumptions, introducing different existing heat sources and taking into account the effect of temperature and pressure on fluid properties (Viscosity, Mud weight, Specific heat), then solve the model using the FINITE ELEMNTS method. Calculations are assisted by MATLAB. The final results will be verified and compared with an analytical solution if possible, or with an existing result of a chosen model. (or with the results obtained using SCHLUMBERGER 'software: DRILL BENCH).

1.4. Thesis structure

The chief aim of this thesis is to have a good prediction of drilling fluid distribution inside a wellbore. We opted for the following structure to let the reader, after finishing the examination of it, not only get a knowledge of the basic principles and theories used to obtain the results, but also to have the possibility to deepen into details that are unlikely to be found in other documents and publications.

An introduction of the drilling operation is presented in the first chapter with a proper description of the problem: Temperature distribution of the drilling fluid during a transient state. The first chapter contains also the most known works realized in this direction, showing that the work done here is an inclusive one, aiming to have the most realistic results with less errors.

The second chapter treats the physical principles and assumptions used to derive the mathematical model in order to obtain the desired results. Different heat sources and heat transfer formulas are given in details, accompanied with the physical laws used to derive the equations. The solution of these equations, requiring a pure knowledge of mathematics, is presented with sufficient details beginning with the main differential equations and the initial and boundary conditions, mentioned at the end. All of this is considered the base for the mathematical work done in the next chapter.

In the third chapter, the discretization of the equations and the initial and boundary conditions are presented. The matrices found after the discretization are impossible to solve manually and MATLAB is needed. The 3$^{\text{rd}}$

chapter includes also the MATLAB code used to solve the matricial system and find the temperature distribution and many other parameters. The last section contains a model verification and that by comparing the obtained results with other well trusted model's results.

Chapter 4 ends the work by presenting the temperature distribution and other outputs when changing input parameters values. The study mainly shows what parameters impact the temperature distribution most. It is also driven to make sure that the MATLAB code responds correctly to the variation of input parameters.

Chapter 02: Physical and mathematical modeling of the problem

Introduction

Heat transfer is the process of the movement of energy due to a temperature difference. Typically, heat loss is proportional to a temperature gradient (driving force or potential). Heat transfer can be achieved by conduction, convection or radiation.[1] The variation of drilling fluid's temperature is due to the heat transfer inside the fluid (Internal Heat transfer), heat extracted from the outer environment (External heat transfer), variation of the fluid internal energy with time (Internal Energy Variation) and to another factor: Variation of fluid 'properties with temperature (Fluid properties variation). Determining all those factors impacting the mud's temperature is primordial to obtain a good prediction of the temperature.

In this chapter, different heat transfer theories will be presented, in addition to fluid properties 'models (Density, Viscosity) used to predict their values in function of temperature and pressure, correlations for the calculations of HTC (Heat transfer coefficients) and also an estimation of the external heat sources. The governing equations of temperature inside the pipe and the annulus are presented at the end of the chapter.

2.1. Internal heat transfer

During the circulation of the fluid, the heat passes from volume element to another by two means:

2.1.1 Thermal conduction

Vertical: As mentioned above, conduction is a way to transport energy (heat). Conduction inside a fluid can be carried out via the THERMAL CONDUCTIVITY property of the fluid (K_f), where the hotter zones will give away energy to the cooler ones. Thus, inside a wellbore, vertical conduction will take place in the ascending direction (From the bottom to the surface). Although, the conduction doesn't have a great impact during circulation, it does at a SHUT-IN situation [2].

To calculate the value of the vertical thermal conduction we use the following expressions [4]:

$$\dot{Q}_{cond\_p}(x,t) = K_f . \pi r_{pi}^2 . \frac{\delta T_p}{\delta x} \tag{2.1}$$

$$\dot{Q}_{cond\_a}(x,t) = K_f . \pi (r_{ci}^2 - r_{po}^2) \frac{\delta T_a}{\delta x} \tag{2.2}$$

Where x represents the depth, t the time, K_f thermal conductivity of the fluid, r_{pi} inner diameter of the drill pipe, r_{po} outer dimeter of the drill pipe, r_{ci} inner diameter of the casing. T_p and T_a are the

temperature of the pipe and the annulus respectively. Finally, $\dot{Q}_{cond\_p}$ and $\dot{Q}_{cond\_a}$ represent the rate of heat transfer via conduction inside the pipe and the annulus respectively.

Radial: In the current study, the radial conduction inside the fluid is neglected, but not between the fluid and the other radial layers of the wellbore. Beginning from the center of the wellbore, the radial layers referred to are: Pipe, drill string, annulus, casing(s), cement(s) and finally the formation.

2.1.2 Mass Transfer

The fluid has a defined rate flow making the mass transfers from the bottom up to the surface. The mass movement induce a heat exchanges where the energy transfers in the same direction the fluid moves (Descending inside the pipe, ascending inside the annulus) . Research found that a small variation of: the specific heat (Cp), the flow rate ($\dot{m}$) and the density (ρ) induce a remarkable alteration on the amount of exchanged heat and therefore a disturbance in the temperature distribution. The expression used is the following [4]:

$$\dot{Q}_m(x,t) = \dot{m}C_pT(x,t) \tag{2.3}$$

Where $\dot{m}$ is the mass flow, C_p the specific heat of the fluid, T the temperature of the mud, and finally $\dot{Q}_m(x,t)$ the rate of heat due to mass transport.

2.2. External heat transfer

This section treats the main heat sources that intervene in the heat exchange process, occurring between a fluid element and the external environment.

2.2.1. Convective heat transfer (Forced convection)

During circulation, since the fluid and the conduit surface have different temperatures, a convective heat transfer will occur.

Close to the wall of a conduit, the fluid's velocity approaches zero and diffusion (conduction) dominates the heat transfer. Here, heat is transferred from the wall surface to the nearby fluid's layer by random molecular motion. The heat going into this layer is transferred further away from the wall by the bulk motion of the fluid (Mass transport), and into the high velocity region. The expression for the convective heat transfer process is given by Newton's law of cooling:

$$q' = h(T_s - T_m) \tag{2.4}$$

where q' is the heat flux, h is the convective heat transfer coefficient (CHTC), T_s and T_m represent the temperature of the conduit surface and the mean fluid's temperature respectively. In terms of the heat transfer process in the wellbore, there exists a convective heat transfer among drill pipe fluid, drill pipe wall, and annulus fluid. The same process occurs among annulus fluid, casing wall, cement layer, and formation. Instead of applying equation (1) to describe these processes individually, an overall heat transfer coefficient (OHTC) is used to consider the net resistance of heat flow over several layers. The convective heat transfer is modeled by the following equations [3]: (see **Kabir et al. (1996)** for more details)

$$Q_{ap} = 2\pi r_{pi} U_p L (T_a - T_p) \tag{2.5}$$

$$Q_{wa} = 2\pi r_{ci} U_a L (T_w - T_a) \tag{2.6}$$

where Q_{ap} and Q_{wa} represent the overall rate of heat transfer from the annulus to the drill pipe and from the formation/wellbore interface to the annulus respectively; r_{pi} is the inner radius of pipe; r_{ci} is the inner radius of casing; T_a and T_p are fluid's temperature inside the annulus and drill pipe respectively; T_w is the wellbore temperature and L is the volume length.[3]

Convective heat transfer coefficient

Overall heat transfer coefficients OHTC, U_p and U_a are defined as follows:

$$\frac{1}{U_p} = \frac{1}{h_p} + \frac{r_{pi}}{k_p} \ln\left(\frac{r_{po}}{r_{pi}}\right) + \frac{1}{h_a} \tag{2.7}$$

$$\frac{1}{U_a} = \frac{1}{h_a} + \frac{r_{ci}}{k_c} \ln\left(\frac{r_{co}}{r_{ci}}\right) + \frac{r_{ci}}{k_{cem}} \ln\left(\frac{r_w}{r_{co}}\right) \tag{2.8}$$

As shown above, OHTCs intervene in determining the heat-transfer rate from a wellbore's mud(inside the annulus) to the surrounding formation during geothermal well drilling operations and also from the mud moving inside the pipe to the mud of the annular section (Beirut, 1991). The OHTC need to be calculated, taking in consideration the Non-Newtonian behavior of the mud (Santoyo, 1997). Research had been driven to estimate accurately the value of the OHTCs in a wellbore. Work was done based on comprehensive rheological evaluation of high-temperature drilling muds. [5

Common correlations for estimating the Nusselt or the Stanton numbers, which intervenes in the estimation of the CHTC (h_p and h_a), appearing in the expressions of the OHTCs, are summarized in **Table 1**. [5]

- The Nusselt number (Nu) is defined as a measure of the heat-flow rate at a fluid/solid interface, i.e., $Nu = \frac{hD}{k}$, where k is the fluid thermal conductivity and D_e is the equivalent diameter, defined respectively in the pipe and the annulus as follows:

$$D_{e\,pipe} = 2r_{pi} \tag{2.9}$$

$$D_{e\,annulus} = 2(r_{ci} - r_{po}) \tag{2.10}$$

By knowing the value of Nu, h_a and h_p can be determined.

- Re is the dimensionless number of Reynolds where $Re = \frac{\rho.V.D_h}{\mu}$

- Pr is the dimensionless number of Prandtl where $Pr = \frac{\mu C_p}{k}$

- St is the dimensionless number of Stanton where $St = \frac{Nu}{Re.Pr}$

- f is the friction coefficient defined in **Table1**.

Forced convection correlation	Literature source	Parameter and flow conditions	
$Nu=0.023Re^{4/5}Pr^n$	Dittus and Boelter (1930)	$0.7 < Pr < 160$ $Re > 10{,}000$ $L/D > 10$	Turbulent flow
$Nu = 0.027Re^{\frac{4}{5}}Pr^{\frac{1}{3}}\left(\frac{\mu}{\mu_s}\right)^{0.14}$	Seider and Tate (1936)	$0.7 < Pr < 16{,}700$ $Re > 5.10^6$ $L/D > 10$	
$Nu = \dfrac{f/8\,(Re - 1000).Pr}{1.07 + 12..7f(Pr^{\frac{2}{3}} - 1)}$	Gnielinski (1976)	$0.7 < Pr < 2000$ $10^4 < Re < 10^6$ $f = (0.79\,lnRe - 1.64)^{-2}$	
$St = 0.071Re^{-0.33}Pr^{-0.67}$	Lakshminarayanan et al. (1976)	$Nu = St.Pe$ $Pe = Re.Pr$	
$Nu = 4.36$	Incropera and DeWitt (1990)	$Re \leq 2300$	Laminar flow

Table 1. *Compilation of the most common empirical correlations for determining the dimensionless Nusselt and Stanton numbers*

2.2.2 Drill pipe rotation

Friction refers to the force that resists relative motion of two solid objects in contact. The mechanical energy released in the process where two solid objects slide against each other is converted to heat. The energy dissipation which is termed frictional heating, results in a temperature increase at the interface between the two objects. In a ***deviated wellbore***, the drill pipe tends to lay at the low side of the wellbore. Consequently, friction occurs at the drill pipe and casing/formation interface and heat is generated during rotation. The frictional force is proportional to the normal force applied by the drill pipe. In highly deviated sections or sharp bends and doglegs where the normal force may be large, an amount of heat can be generated.
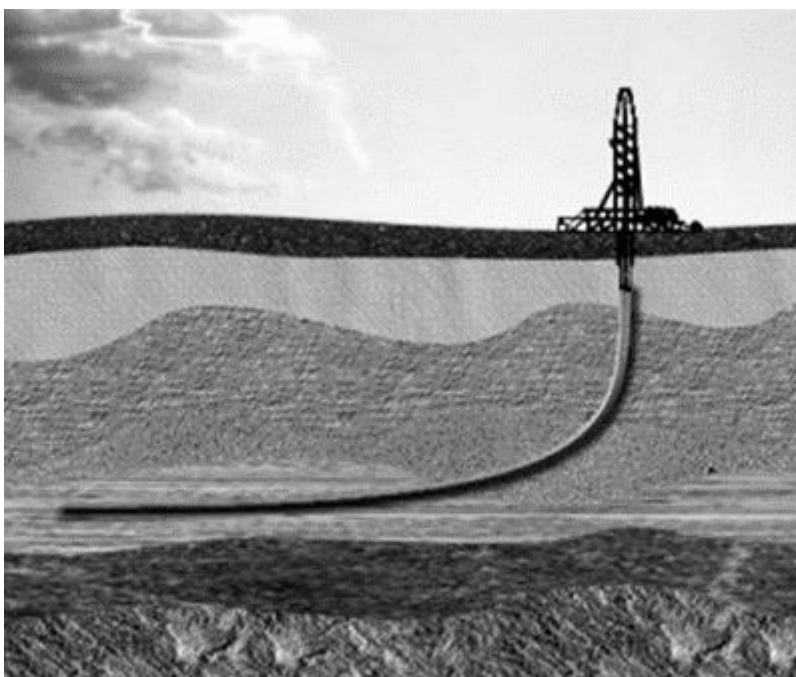
Figure 3. A deviated wellbore

To quantify the amount of heat that is generated because of wellbore friction, the equation proposed by ***Kumar and Samuel (2013)*** is applied in this work:

$$q_p = \tau_p . 2\pi . RPS \tag{2.11}$$

where q_p is downhole power loss, τ_p is the torque acting on the drill pipe due to wellbore friction and RPS represents the drill pipe rotations per second.

In this work, the temperature will be calculated for a vertical wall, meaning that there is no friction between the formation and the drill pipe. q_p will not be taken in consideration.

2.2.3. Bit friction

While the bit is drilling, due to friction at the interface formation/Bit, energy dissipation occurs. The difficulty that exists is to determine the amount of energy dissipation that will be converted into thermal energy. ***Keller et al. (1973)*** stated that only 40% of the energy furnished to rotate the drill pipe is used to crush the rock while ***Corre et al. (1984)*** suggested that only 10 % is used. Those suggestions are not based on scientific researches. Researches driven toward this direction being so scarce, an accurate estimation of the true value of the heat generation is difficult. [3]

Alternatively, mechanical specific energy (MSE) might be a good indicator for having an idea to estimate the heat generated from the bit friction. MSE is a term that gives the energy required to remove a unit volume of rock. It is defined by the general expression in ***Hamrick (2011):***

$$MSE = \frac{Toatal\ energy\ input}{Volume\ removed} = \frac{WOB}{Area} + \frac{2\pi.RPM.\tau_b}{Area.ROP} \qquad (2.12)$$

where WOB is weight on bit (amount of downward force exerted on the drill bit), RPM is rotation per minute of the bit, Area is wellbore area, τ_b is torque bit and ROP is rate of penetration.

The heat generated from penetrating the rock can be possibly estimated as:

$$q_b = \tau_b.2\pi.RPS_b + \delta_b.WOB.ROP \qquad (2.13)$$

Where RPS_b represents Rotation per second of the drill bit, δ_b is the model coefficient to describe the efficiency of the work.

2.2.4 Pressure losses

Close to the wall, the velocity gradient, due to the circulation of the mud, will be large and layers of fluid will move relatively to each other. The friction that occurs between these layers because of fluid viscosity, results in a pressure drop and consequently heat generation during circulation. The heat due to the friction of fluid circulation is given as [3]:

$$q_{pl} = \Delta P.Q \qquad (2.14)$$

where ΔP is the pressure drop, Q is flow rate. The pressure loss estimation method is presented in the section **(2.4.2).**

2.2.5 Joule-Thomson effect

As a liquid or a gas is either compressed or expanded, a subsequent change of temperature is experienced. Whether the temperature decreases or increases depends on the original state of the fluid. To consider this effect in the temperature model, the Joule-Thomson (JT) coefficient is implemented. The JT coefficient describes how the temperature of a fluid is affected by changes in pressure at constant enthalpy, see *Maghari and Safaei (2007).* The change of temperature due to pressure changes is mathematically described as [3]:

$$q_{JT} = mC_p\mu_{JT}\frac{\Delta p}{\Delta x}$$
(2.15)

where μ_{JT} is the JT coefficient. The approach in Alves et al. (1992) has been employed to calculate the JT coefficient for the drilling fluid as:

$$\mu_{JT} = \frac{1}{C_p}\left[T\left[\frac{\partial}{\partial T}\left(\frac{1}{\rho}\right)\right]P - \frac{1}{\rho}\right]$$
(2.16)

2.3 Thermal energy

Giving that this work is meant to study the variation of mud's temperature during transient state, the time factor should be integrated. All the heat exchanges explained earlier cause an alteration in the internal energy of the fluid, which is the energy contained within it. The energy of a fluid element depends directly on one most important factor among so many others: *Fluid temperature.* The more the fluid is exposed to heat, the more its temperature changes and vice-versa, following the relation mentioned above:

$$\frac{\partial E}{\partial t} = \frac{\partial(mC_pT)}{\partial t}$$
(2.17)

As equation (2.17) demonstrates, both temperatures at *t* (Present state) and *t-dt* (Previous state) affects the Internal energy at the moment *t*. Knowing the previous state of the fluid is primordial to know the current state.

2.4 Temperature and pressure dependent rheological parameters

The rheology or flow behavior of most drilling fluids is non- Newtonian. For this study, a Bingham plastic model was employed to express the flow behavior of drilling fluids. The Bingham plastic model can be expressed as follows [10]:

$$\tau = \tau_0 + \mu_p \gamma \tag{2.18}$$

Where τ is shear stress τ_0 is the yield stress, μ_p is plastic viscosity and γ is the shear rate. In order to analyze the flow behavior of drilling fluids under high pressure-high temperature conditions, the following variation on the Bingham-plastic model developed by Politte1 was employed.

2.4.1 Plastic Viscosity model

Politte1 analyzed rheological data for diesel-based drilling and found the plastic viscosity tracked the behavior of the base oil. Hence, the plastic viscosity was normalized with the viscosity of the base oil. The steps of the method are detailed as follows:

1. Measure plastic viscosity of the drilling fluid at standard conditions.
2. Measure base oil viscosity at standard conditions and at the pressure and temperature of interest.
3. Calculate plastic viscosity of the drilling fluid at the conditions of interest as follows:

$$\mu_p(P,T) = \mu_{p\,0} \cdot \frac{\mu(P,T)}{\mu_0} \tag{2.19}$$

Politte obtained the following expression for the base oil viscosity as a function of temperature and pressure from analysis of diesel oil [10]:

$$\mu(T,P) = P * (T * P)^{A_0} \cdot 10^{\left(A_1 + A_2 T + A_3 TP + A_4 P + A_5 \rho + \frac{A_6}{\rho}\right)} \tag{2.20}$$

$$A_0 = -23.1888\,,$$
$$A_1 = -0.00148,$$
$$A_2 = -0.9501,$$
$$A_3 = -1.9776.10^{-8},$$
$$A_4 = 3.3416.10^{-5},$$
$$A_5 = 14.6767$$

$$A_6 = 0.089$$

Where A0, A1, A2, A3, A4, A5, and A6 are empirical constants, and ρ is the base oil density as a function of temperature. This is evaluated from the next **section (2.4.3 Density model)**

2.4.2 Pressure loss estimation

The loss in pressure during flow, is a result of contact between the drilling fluid and the walls of the flow conduit. A boundary layer is formed along the surface of a flow conduit carrying a fluid. The viscous property of the fluid creates a variation in the flow velocity normal to the direction of flow. This variation in fluid velocity represents a loss in momentum and a resistance to flow. The associated pressure loss is directly proportional to the length of the flow conduit, the fluid density, and the square of the fluid velocity, and is inversely proportional to the conduit diameter.

$$\Delta P = \frac{f_d \rho V^2 L}{2D} \tag{2.21}$$

Where ρ is the fluid density, V is the fluid velocity, L is the length of the flow conduit, D_{pi} is the pipe diameter, and f is known as the fanning friction factor. In the case of noncircular flow conduits like the annulus, the diameter is replaced by the equivalent diameter.

$$d_e = 4\frac{A_c}{P_w} \tag{2.22}$$

Where d_e is the equivalent diameter, A_c is the cross-sectional area of the flow conduit, and P_w is the wetted perimeter.

Determining the yield point

Politte concluded from his analysis of rheological data for emulsions that drilling fluid yield point is not a strong function of pressure. The effects of temperature on the yield point however, are difficult to predict. Politte provides the following steps to know the true behavior of the drilling fluid. They are based on an empirical equation obtained from analysis of diesel oil-based drilling fluid [10]:

- Measure yield point at standard conditions.
- Calculate the yield point of the drilling fluid at the temperature of interest using the following equation:

$$\tau_y = \tau_{yo} \frac{B_0 + B_1 T^{-1} + B_2 T^{-2}}{B_0 + B_1 T_0^{-1} + B_2 T_0^{-2}} \tag{2.23}$$

$$90°F \leq T \leq 300F°$$

$$B_0 = -0.186, \qquad B_1 = 145.054, \qquad B_2 = -3410.322$$

Where τ_{yo} is the yield point at reference temperature, τ_y is the yield point at elevated temperature, and B0, B1, and B2 are empirical constants.

Determining the pressure loss

In order to calculate frictional pressure loss, it must be determined if the flow regime is laminar or turbulent. This is done by calculating the Reynolds number according to the following equation:

$$N_{Re} = \frac{928 \rho \bar{V} d}{\mu_a} \tag{2.24}$$

Where:

ρ: Fluid density (lb./gal)

$\bar{V}$: Average fluid viscosity(ft/s)

d: Pipe diameter or equivalent annular diameter (In)

μ_a: Apparent viscosity(cp)

Laminar flow

A Reynolds number at or below 2100 indicates laminar flow. A Reynolds number greater than 2100 indicates turbulent flow. If the flow is laminar, the frictional pressure drop is calculated according to the following equations based on the Bingham plastic model.[10]

Pipe

$$\Delta P = \left(\frac{\mu_p \bar{V}}{1500 \, D_{pi}^2} + \frac{\tau_y}{225 D_{pi}} \right) \Delta L \tag{2.25}$$

The apparent viscosity is calculated according to the following equations derived from the Bingham plastic model.

$$\mu_a = \mu_p + \frac{6.66 \tau_y D_{pi}}{\bar{V}} \tag{2.26}$$

D_{pi} is the inner diameter of the pipe.

Annulus

$$\Delta P = \left(\frac{\mu_p \bar{V}}{1500 (D_{ci}^2 - D_{po}^2)} + \frac{\tau_y}{200 (D_{ci} - D_{po})} \right) . \Delta L \tag{2.27}$$

The apparent viscosity is calculated according to the following equations derived from the Bingham plastic model.

$$\mu_a = \mu_p + \frac{5 \tau_y d_e}{\bar{V}} \tag{2.28}$$

D_{ci} is the inner diameter of the casing, D_{po} is the outer diameter of the pipe.

Turbulent Flow

If the flow is turbulent, the friction factor is calculated according to the Colebrook equation as follows[10]:

$$\frac{1}{\sqrt{f}} = 4 \log_{10}(N_{Re}\sqrt{f}) - 0.395 \tag{2.29}$$

The friction factor is then used in **Eq (2.21)** to calculate the frictional pressure loss.

2.4.3 Density model

Fluid density

Density, or what we call in industry mud weight is measured in field using mud scale or mud balance. Mud weight is used to control the trapped fluids or gas in the formations by adding a hydro static pressure on them. If the hydro static pressure increased over the formations pressure that will make a fracture in the formation leading to lose the mud to the formation, so adding loss circulation material like gel-flake or wood chips that can refill the gap and stop the mud loss. If the mud loss continues, then the hydro static pressure will decrease and flammable fluids and gas trapped under pressure will start leaking to the surface. This can lead to a potential Blow-out.[11]

Due to their immiscible behavior, the total volume of the mud is equal to the sum of the volume of every component, assuming that the mixture is homogenous. It is called an ideal mixture.

$$V_f = V_w + V_o + V_{ls} + V_{hs} \tag{2.30}$$

where V_f is the total fluid volume, V_w is the volume of the water phase, V_o is the volume of the oil phase, V_{ls} is the volume of the low-density solids, and V_{hs} is the volume of the high-density solids.

The mass of a volume V_f of mud is equal to the sum of the masses of the components:

$$m_f = \rho_w.V_w + \rho_o.V_o + \rho_{ls}V_{ls} + \rho_{hs}V_{hs} \tag{2.31}$$

Where m_f is the mass of the fluid mixture, ρ_w is the density of the water phase, ρ_o is the density of the oil phase, ρ_{ls} is the density of the low-density solids, and ρ_{hs} is the density of the high-density solids.
The total density of the mud is defined:

$$\rho_f = \rho_w.f_w + \rho_o.f_o + \rho_{ls}f_{ls} + \rho_{hs}f_{hs} \tag{2.32}$$

Where f_w is the volume fraction of the water phase, f_o is the volume fraction of the oil phase, f_{ls} is the volume fraction of the low-density solids, and f_{hs} is the volume fraction of the high-density solids.

While the solid phases show little change over typical ranges of temperature and pressure, water does show some change with temperature, and oil shows considerable change with pressure and temperature. Water is relatively incompressible, while oils are much more compressible. If we review **Eq. (2.30),** we see that the volume of the fluid changes as the volume of the water phase and oil phase changes. As a result, the volume fractions, computed at a given pressure and temperature, are not constants and vary with changes in pressure and temperature. If we measure volume fractions at a specified temperature, the following formula gives the density of the mixture at new temperatures and pressures:

$$\rho_f = \frac{\rho_f(P,T)}{1 - \frac{f_o \Delta \rho_o}{\rho_o(P,T)} - \frac{f_w \Delta \rho_w}{\rho_w(P,T)}} \qquad (2.33)$$

Where

$$\Delta \rho_o = \rho_o(P,T) - \rho_o(P_r,T_r) \qquad (2.34)$$

$$\Delta \rho_w = \rho_w(P,T) - \rho_w(P_r,T_r) \qquad (2.35)$$

Where P_r and T_r are the reference pressure and temperature used to calculate the fractions f_w and f_o[12].

Water and oil density

For a precise analytical formula of water density, we recommend the following correlation:

$$\rho_w = 8.63186 - 3.31977.10^{-3}T + 2.37170.10^{-5}P \qquad (2.36)$$

Where ρ_w is the density of water in lbm/gal, T is the temperature in °F and P is the pressure in psia.
A general correlation for the density of oil is given by:

$$\rho_o = 8.3154[(a_0 T + B_0) + (a_1 T + b_1)P + (a_2 T + b_2)P^2] \qquad (2.37)$$

Where ρ_o is the density of oil in lbm/gal, T is the temperature in °F and P is the pressure in psia.
The following table gives the values of a_0, a_1, a_2, b_0, b_1 and b_2 for a synthetic oils and Diesel.

	$a_0 \times 10^4$	$b_0 \times 10$	$a_1 \times 10^8$	$b_1 \times 10^{16}$	$a_2 \times 10^{13}$	$b_2 \times 10^{12}$
Diesel	-3.6058	8.7071	0.4640	3.6031	-1.6843	-72.465
LVT 200	-3.8503	8.3847	1.5695	2.4817	-4.3373	6.5076
LAO C16C18	-3.5547	8.1304	1.2965	3.1227	-2.7166	-28.894
Saraline 200	-3.7621	8.0019	1.5814	2.3560	-4.3235	10.891
EMO-4000	-3.7799	8.4174	1.3525	2.8808	-3.1847	-17.697

Table 2- Coefficients for oil density correlation

PVT model

In order to avoid the repetition of all the stages explained previously, one can use a correlation for the calculation of the density of the drilling fluid at any temperature and pressure. The correlation is linear in temperature and quadratic in pressure and it takes the following form:

$$\rho_f = (A_0 T + B_0) + (A_1 T + B_1)P + (A_2 T + B_2)P^2$$

(2.38)

Fluid composition

The studied fluid is an oil base type with 100% Diesel, and Barite as the high-density solids without water nor low density solids, we use this drilling fluid for all the simulations to come.

The reference temperature and pressure are: $P_r = 0\ Psi\ ,T_r = 60°F$

The density of the drilling fluid at the reference temperature and pressure ($0\ psi, 60\ °F$) is 2500 kg/m^3.

After calculating the drilling fluid density using **Eq (2.33)**, we can interpolate the results to find the coefficients $A_{i=0,1,2}$ and $B_{i=0,1,2}$ in **Eq (2.38)**. The results are presented in **Table 2**.

A_0	-4.59×10^{-04}	B_0	1.226
A_1	$6..38 \times 10^{-09}$	B_1	4.49×10^{-06}
A_2	-2.26×10^{-13}	B_2	-9.07×10^{-11}

Table 3- *Coefficients for the drilling fluid density correlation*

2.5. Derivation of the temperature model

In order to simulate temperature in and around a wellbore during drilling phases, the model need to take into account several features: [6]

- An evolutive geometry at the level of the tool.
- Fast changing operating conditions.
- Heat source terms generated by pressure losses and rotational energy (mentioned earlier).

2.5.1 Governing equations inside the pipe

Inside the pipe, mud is travelling from the inlet surface toward the bottom. During the circulation, a volume element of the fluid extracts energy by forced convection from its adjacent volume element in the annulus. Mass transport plays a role in determining the amount of heat getting in the Volume Element and going out of it. Temperature variation is also due, to a lesser extent, to vertical conduction within the liquid (Except during shut-in where the conduction is important).[2]

Using the first law of thermodynamics for a control volume, the temperature model should be found.

First law of thermodynamics:

$$d\dot{Q} - d\dot{W} = d\dot{E} + dh \tag{2.39}$$

where dh is the variation of enthalpy, $\dot{E}$ is the variation of internal energy, $\dot{W}$ is the work furnished to the system (here equal to 0), $\dot{Q}$ is the heat transfer.

Using the definitions presented in the previous chapter, we find that:

Mass transport:

$$dh = h(x,t) - h(x+dx,t) = [\dot{m}C_pT](x,t) - [\dot{m}C_pT](x+dx,t) = -\frac{\partial(\dot{m}C_pT)}{\partial x}.\ dx \tag{2.40}$$

Using discretization, we find:

$$h_i - h_o = h(x_{j-1},t) - h(x_j,t) = \dot{m}C_pT_{j-1}^{n+1} - \dot{m}C_pT_j^{n+1} \tag{2.41}$$

Thermal conduction:

$$dQ_{cond} = Q_{cond}(x,t) - Q_{cond}(x-dx,t) = [K_f . S_0 \frac{\partial T}{\partial x}](x,t) - [K_f . S_0 \frac{\partial T}{\partial x}](x-dx,t)$$

$$= \frac{\partial}{\partial x}[K_f . S_0 \frac{\partial T}{\partial x}](x,t) \tag{2.42}$$

Where $S_0 = \pi r_{ci}^2$ the section of the pipe. Using discretization, we find:

$$Q_{cond_t} = Q_{cond}(x_j, t) - Q_{cond}(x_{j-1}, t) = K_f . \pi r_{ci}^2 . \left(\frac{T_{j+1}^{n+1} - T_j^{n+1}}{\Delta x}\right) - K_f . \left(\frac{T_j^{n+1} - T_{j-1}^{n+1}}{\Delta x}\right)$$

$$= K_f . S_0 (\frac{T_{j+1}^{n+1} - 2T_j^{n+1} + T_{j-1}^{n+1}}{\Delta x}) \tag{2.43}$$

Forced convection:

$$dQ_{ap} = 2\pi r_{pi} U_p dx \left(T'(x,t) - T(x,t)\right) \tag{2.44}$$

Using discretization, we find :

$$Q_{ap} = 2\pi r_{pi} U_p \Delta x \left(T_j'^{(n+1)} - T_j^{n+1}\right) \tag{2.45}$$

Where $T_j'^{(n+1)}$ refers to the temperature of the annulus fluid at node j at the moment $t = t_0 + (n+1)\Delta t$, and T_j^{n+1} refers to the temperature of the pipe fluid at the nod j at the moment $t = t_0 + (n+1)\Delta t$.

Internal energy:

$$d\dot{E} = dm . C_p \frac{\partial T}{\partial t}(x,t) \tag{2.46}$$

$$dm = \rho . 2\pi r_{ci} . dx.$$

Using discretization, we find:

$$\Delta \dot{E} = \rho . 2\pi r_{ci} . \Delta x . C_p (\frac{T_j^{n+1} - T_j^n}{\Delta t}) \tag{2.47}$$

Energy sources

$$dQ_p(x,t) = dQ_{pl}(x,t) - dQ_{JT}(x,t) \qquad (2.48)$$

$$Qp_j^{n+1} = Q_{pl}{}_j^{\,n} - Q_{JT}{}_j^{\,n} \qquad (2.49)$$

Final equation:

By substitution of the equations (3.2), (3.3), (3.4), (3.5), (3.6) into (3.1), the following equation is found:

$$\boldsymbol{Q_p} + \frac{\partial}{\partial x}\left[K_f.S_0.\frac{\partial T}{\partial x}.dx \right] - \frac{\partial(\dot{m}C_p T)}{\partial x}.dx + 2\pi r_{pi}U_p dx(T'-T) = dm.C_p\frac{\partial T}{\partial t} \qquad (2.50)$$

Boundary conditions

- The inlet temperature of the mud can be modeled by a time function. Depending on operating conditions, this function is determined. The different models used in the industry are presented in the next section of this chapter (Section 2.6).

$$T_{in} = T_{in}(t)$$

2.5.2 Governing equations inside the annulus

For the annular section, the fluid comes from the bottom of the well and travels back to the tanks at the surface. This mass transport and heat exchange with the formation, as well as with pipe's fluid contributes in the changes of temperature. The different heat sources affect temperature distribution also. All those factors will be modeled using the following equations.

Mass transport

$$h_i(x,t) - h_o(x,t) = dh = h_f(x+dx,t) - h_f(x,t) = \left[\dot{m}C_p T'\right](x+dx,t) - \left[\dot{m}C_p T'\right](x+dx,t)$$

$$= \frac{\partial(\dot{m}C_p T')}{\partial x}.dx \quad (3.8) \qquad (2.51)$$

Thermal conduction

$$dQ_{cond} = Q_{cond}(x,t) - Q_{cond}(x-dx,t) = [K_f.S_1\frac{\partial T'}{\partial x}](x,t) - [K_f.S_1\frac{\partial T'}{\partial x}](x-dx,t)$$

$$= \frac{\partial}{\partial x} [K_f . S_1 \frac{\partial T'}{\partial x}] dx(x,t) \tag{2.52}$$

Where $S_1 = \pi(r_{ci}^2 - r_{po}^2)$

Forced convection

$$dQ_{pa} = 2\pi r_{pi} U_p dx(T - T') \tag{2.53}$$

$$dQ_{wa} = 2\pi r_{ci} U_a dx(T_w - T') \tag{2.53}$$

Internal energy

$$d\dot{E} = dm.C_p \frac{\partial T'}{\partial x}(x,t) \tag{2.54}$$

Where $dm = \rho.2\pi(r_{ci}^2 - r_{po}^2).dx$.

Energy sources

$$dQ_a(x,t) = dQ_{pl}(x,t) + dQ_{JT}(x,t) + dQ_b(x,t). \tag{2.55}$$

Final equation

By substitution of the equation (3.8), (3.9), (3.10), (3.11), (3.12), (3.13) into (3.1), the following equation is found:

$$\boldsymbol{Q_a} + \frac{\partial}{\partial x} [K_f . S_1 . \frac{\partial T'}{\partial x} . dx] + \frac{\partial(\dot{m}C_p T')}{\partial x} . dx + 2\pi r_{pi} U_p L(T - T') + 2\pi r_{ci} U_a L(T_w - T') = dm.C_p \frac{\partial T'}{\partial t} \tag{2.56}$$

Boundary conditions:

- The Dirichlet conditions as mentioned by *Saedi et al. (2018)* for the bottom hole is used in this work and is written as follows:

$$T_a(x_{max}, t) = T_p(x_{max}, t) \tag{2.57}$$

2.5.3 Governing equations of the formation

The temperature of the formation changes due to the heat exchange with the annulus. The heat exchange between them is radial convection. To determine the radial distribution of the temperature inside the formation, determining the heat exchanges and boundary conditions are necessary.

Inside a control volume of formation, radial conduction occurs, and the internal energy of the formation varies with time. No other heat sources intervene in determining the temperature. The governing equation of the formation is given by the following expression:

$$\frac{1}{r}\frac{\partial}{\partial r}\left(r\frac{\partial T_f(r,x,t)}{\partial r}\right) = \frac{1}{\alpha}\frac{\partial T_f(r,x,t)}{\partial t} \tag{2.58}$$

Boundary conditions are needed at the interface wellbore/formation and at $r \to \infty$.

At the interface wellbore/formation, the convective heat transfer with the annulus is equal to zero:

$$Q_{cond}(r = r_w, x, t) = 0 \tag{2.59}$$

Heat exchange between the formation and annulus is governed by the following equation.

$$2\pi r_w k_f \frac{\partial T_f(x,r_w,t)}{\partial r} - 2\pi r_w U_a \left(T_f(x,r_w,t) - T_a(z,t)\right) = 2\pi r_w Dr\rho C_{for}\frac{\partial T_f(x,r_w,t)}{\partial r} \tag{2.60}$$

The more the point from the formation where the temperature is calculated is far from the wellbore, the less its temperature is affected by the contact of the formation with the annulus and tends to have stability by taking the values of the geothermal conditions after reaching a definite distance from the well.

At $r \to \infty$, the defined boundary condition is the following:

$$T_f(r,x,t) = T_{geothermal}(Z) \tag{2.61}$$

The geothermal temperature is defined along X axis by:

$$T_{geothermal}(x) = T_{f0} + G.x \tag{2.62}$$

Where T_{f0} is the formation temperature at the surface of the earth, G is the geothermal gradient and x is the depth.

2.6 Pressure calculation

The pressure calculation in the annular section and the pipe are given as follows :

Annular flow:

Flow section

$$S_{a(i)} = \pi(r_{ci(i)}^2 - r_{po(i)}^2)$$

(2.63)

Annulus flow velocity

$$v_{a(i)} = \frac{Q}{S_{a(i)}}$$

(2.64)

Hydraulic diameter

$$D_{ha(i)} = 2(r_{ci(i)} - r_{po(i)})$$

(2.65)

Effective diameter

$$D_{ea(i)} = \frac{3nD_{ha(i)}}{2n + 1}$$

(2.65)

Reynolds number

$$Re_{a(i)} = \frac{D_{ea(i)}\rho_{a(i)}v_{a(i)}}{\mu_{aa(i)}}$$

(2.66)

Hydrostatic pressure

$$P_{ha(i)} = \rho_{a(i)}.g.(x_i - x_{i-1}) + P_{ha(i-1)}$$

(2.67)

$P_{ha(0)}$ is known and we can set it equal to 0 Pa for example.

Reynolds number at laminar flow boundary:

$$Re_{lam} = 3470 - 1370.n$$

(2.68)

Reynold number at turbulent flow boundary:

$$Re_{tur} = 4270 - 1370.n$$

(2.69)

Friction factor

Friction factor has different expressions, depending on the flow regime (laminar, transitional, turbulent):

Laminar: $\quad f_{a(i)} = \dfrac{24}{Re_{a(i)}} \qquad Re_{a(i)} \leq Re_{lam}$

Transitional : $f_{a(i)} = \left(\dfrac{24}{Re_{lam}}\right) + \left(\dfrac{Re_{a(i)} - Re_{lam}}{800}\right) \times \left(\left(\dfrac{a}{Re_{tur}^b}\right) - \left(\dfrac{24}{Re_{lam}}\right)\right) \qquad Re_{lam} < Re_{a(i)} \leq Re_{tur}$

Turbulent : $\quad f_{a(i)} = \dfrac{a}{Re_{tur}^b} \qquad Re_{tur} < Re$

Where

$$a = \frac{\log_{10}(n) + 3.93}{50}$$

$$b = \frac{1.75 - \log_{10}(n)}{7}$$

Pressure loss

$$\Delta P_{a(i)} = \left(\frac{f_{a(i)} \cdot \rho_{a(i)} \cdot \left(v_{a(i)}\right)^2}{2 D_{ha(i)}}\right)(x_i - x_{i-1}) \tag{2.70}$$

Cumulative pressure loss

$$PL_{cum,a(0)} = \Delta P_{a(0)} \tag{2.71}$$

$$PL_{cum,a(i)} = PL_{cum,a(i)} + \Delta P_{a(i)} \tag{2.72}$$

Dynamic pressure

$$P_{da(i)} = P_{ha(i)} + PL_{cum,a(i)} \tag{2.73}$$

Pipe flow:

Flow section

$$S_{p(i)} = \pi \cdot r_{pi(i)}^2 \tag{2.73}$$

Annulus flow velocity

$$v_{p(i)} = \frac{Q}{S_{p(i)}} \tag{2.74}$$

Hydraulic diameter

$$D_{hp(i)} = 2.r_{pi(i)} \tag{2.75}$$

Effective diameter

$$D_{ep(i)} = \frac{4nD_{ha(i)}}{3n+1} \tag{2.76}$$

Reynolds number

$$Re_{a(i)} = \frac{D_{ep(i)}\rho_{p(i)}v_{p(i)}}{\mu_{ap(i)}} \tag{2.77}$$

Hydrostatic pressure

$$P_{hp(i)} = \rho_{p(i)}.g.(x_i - x_{i-1}) + P_{hp(i-1)} \tag{2.78}$$

$P_{ha(0)}$ is known and we can set it equal to 0 Pa for example.

Reynolds number at laminar flow boundary:

$$Re_{lam} = 3470 - 1370.n \tag{2.79}$$

Reynold number at turbulent flow boundary:

$$Re_{tur} = 4270 - 1370.n \tag{2.80}$$

Friction factor

Friction factor has different expressions, depending on the flow regime (laminar, transitional, turbulent):

Laminar: $f_{a(i)} = \frac{24}{Re_{a(i)}}$ $Re_{a(i)} \leq Re_{lam}$

Transitional : $f_{a(i)} = \left(\frac{24}{Re_{lam}}\right) + \left(\frac{Re_{a(i)} - Re_{lam}}{800}\right) \times \left(\left(\frac{a}{Re_{tur}^b}\right) - \left(\frac{24}{Re_{lam}}\right)\right)$ $Re_{lam} < Re_{a(i)} \leq Re_{tur}$

Turbulent : $f_{a(i)} = \frac{a}{Re_{tur}^b}$ $Re_{tur} < Re$

Where

$$a = \frac{\log_{10}(n) + 3.93}{50}$$

$$b = \frac{1.75 - \log_{10}(n)}{7}$$

Pressure loss

$$\Delta P_{p(i)} = \left(\frac{f_{p(i)} \cdot \rho_{p(i)} \cdot \left(v_{p(i)} \right)^2}{2 D_{hp(i)}} \right) (x_i - x_{i-1}) \tag{2.81}$$

Cumulative pressure loss

$$PL_{cum,a(0)} = \Delta P_{p(0)} \tag{2.82}$$

$$PL_{cum,p(i)} = PL_{cum,p(i)} + \Delta P_{p(i)} \tag{2.83}$$

Dynamic pressure

$$P_{dp(i)} = P_{hp(i)} + PL_{cum,p(i)} \tag{2.83}$$

Conclusion

The governing equations of the temperature inside the pipe, the annulus and the formation were presented in detail in this chapter. Pressure calculations were given, due to its impact on the rheological properties of the fluid. The solution of these equations requires a knowledge of numerical resolution methods, since the analytical solution isn't available. The next chapter will finish the work done earlier and will transfom these equations from non-linear to linear, making it easy to solve them algebraically.

Chapter 3: Discretization and MATLAB code presentation

Introduction

From the previous chapters, all the inputs of the current model were presented with deep detail. This chapter includes the method used to find the outputs of the model, basically the temperature distribution. The non-linear equations are discretized in finite difference fully implicit scheme and solved by the Newton's method. The choice of the implicit method is due to its numerical stability and its convergence, although it is more numerically intensive than the explicit method.[13] The resolution of the obtained matrixial system is completed using a MATLAB code. The model will be validated comparing its results to the actual literature and results obtained from an established software.

3.1 Numerical approach

3.1.1 Discretized equations

Our goal is to find approximate solutions to differential equations since the exact solution that only an analytical method can give is not available. A finite difference method proceeds by replacing the derivatives in the differential equations by finite difference approximations. This gives a large algebraic system of equations to be solved instead of the differential equation, something that is easily solved using MATLAB. In the following, the approximations of the derivatives of temperature function $T(x, t)$ by finite difference formulas based only on values of temperature at discrete points are presented.

- **First order derivatives** $\quad \frac{\partial T}{\partial x}(x_i, t_n) \cong \frac{T(x_{i+1}, t_n) - T(x_i, t_n)}{Dx} = \frac{T_{i+1}^n - T_i^n}{\Delta x}$ (3.1)

- **Second order derivatives** $\quad \frac{\partial^2 T}{\partial x^2}(x_i, t_n) \cong \frac{T(x_{i+1}, t_n) - 2T(x_i, t_n) + T(x_{i-1}, t_n)}{(Dx)^2} = \frac{T_{i+1}^n - 2T_i^n + T_{i-1}^n}{(\Delta x)^2}$ (3.2)

- **First order derivatives** $\quad \frac{\partial T}{\partial t}(x_i, t_n) \cong \frac{T(x_i, t_{n+1}) - T(x_i, t_n)}{Dt} = \frac{T_i^{n+1} - T_i^n}{\Delta t}$ (3.3)

Where Δx is the length step, Δt is the time step, T_i^n is the temperature of the fluid(pipe or annulus) at a depth $x_i = i.\Delta x$, and a time of $t_n = n.\Delta t$.

The notation of the discretized wellbore is given in **Fig 5.**

By implementing the definitions **Eq (3.1), (3.2), (3.3)** into the governing equations of pipe, anulus and formation temperature, the following discretized equations will be found

Pipe:

$$a T_{p(j)}^{n+1} + b T_{p(j-1)}^{n+1} + c T_{p(j+1)}^{n+1} + d T_{p(j)}^{n} + e T_{a(j)}^{n+1} = F_{p(j)}^{n+1} \qquad (3.5)$$
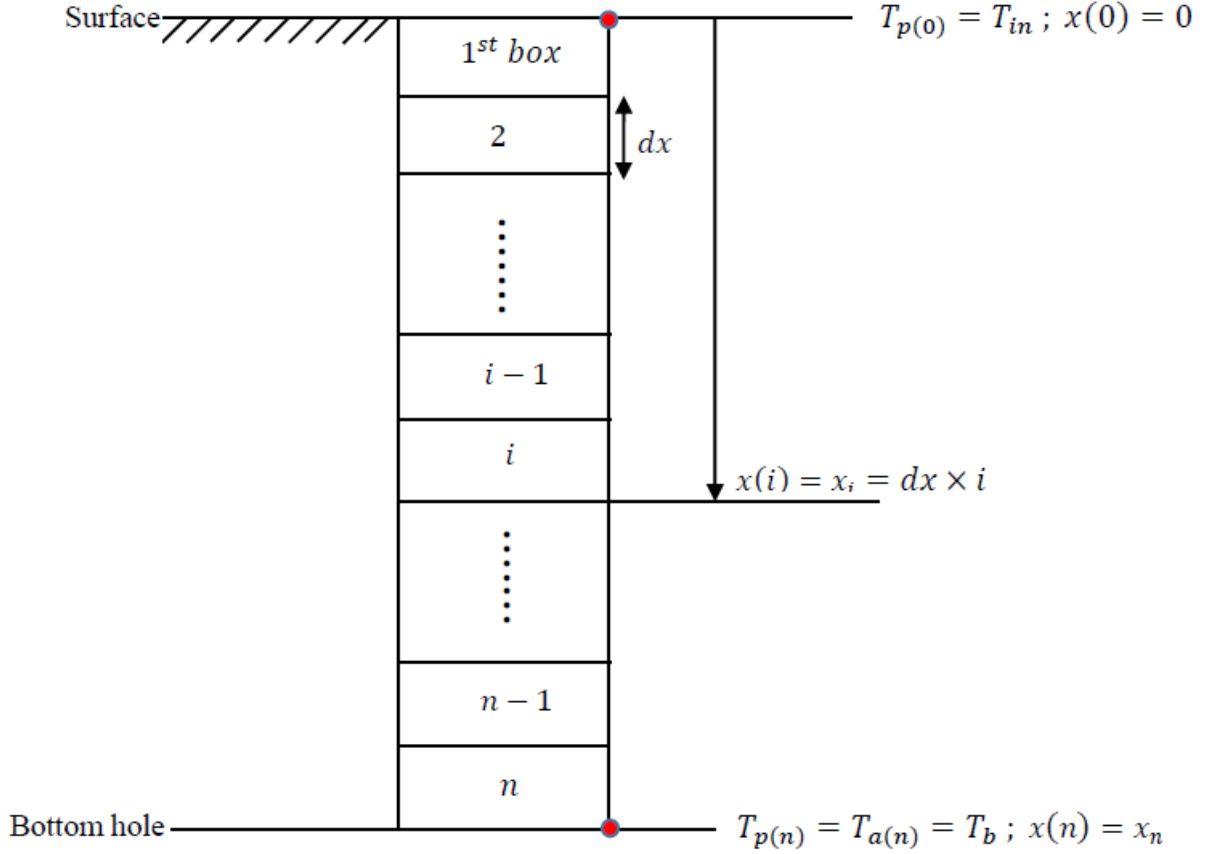
Figure 4. Discretized wellbore

The coefficients of the **Eq (3.5)** are given as follows

$$
\begin{cases}
a = \dot{m} C p + \dfrac{2 K_f \pi r_{ip}^2}{Dx} + \dfrac{\rho \pi r_{ip}^2 Dx C_p}{Dt} + 2 \pi r_{ip} Dx U_p \\[2mm]
b = -\dot{m} C p - \dfrac{K_f \pi r_{ip}^2}{Dx} \\[2mm]
c = -\dfrac{K_f \pi r_{ip}^2}{Dx} \\[2mm]
d = \dfrac{\rho \pi r_{ip}^2 Dx C_p}{Dt} \\[2mm]
e = -2 \pi r_{ip} Dx U_p \\[2mm]
F_{p(j)}^{n+1} = Q_{pl\,j}^{n+1} - Q_{JT\,j}^{n+1}
\end{cases}
$$

Where $\dot{m}$ is the mass flow rate, Cp is the fluid heat capacity, K_f is the fluid heat conductivity, r_{ip} is the inner radius of the pipe, U_p is the overall heat transfer coefficient between the pipe and the annulus.

Annulus:

$$a_0 T_{a(j)}^{n+1} + b_0 T_{a(j-1)}^{n+1} + c_0 T_{a(j+1)}^{n+1} + d_0 T_{a(j)}^{n} + e_0 T_{p(j)}^{n+1} + g_0 T_{j,1}^{n+1} = F_{a(j)}^{n+1} \tag{3.6}$$

The coefficients of the **Eq (3.6)** are given as follows:

$$\begin{cases} a_0 = \dot{m}Cp + \dfrac{2K_f\pi\left(r_{ic}^2 - r_{op}^2\right)}{Dx} + \dfrac{\rho\pi(r_{ic}^2 - r_{op}^2)DxC_p}{Dt} + 2\pi r_{ip}DxU_p + 2\pi r_w DxU_a \\[2mm] b_0 = -\dfrac{K_f\pi\left(r_{ic}^2 - r_{op}^2\right)}{Dx} \\[2mm] c_0 = -\dot{m}Cp - \dfrac{K_f\pi\left(r_{ic}^2 - r_{op}^2\right)}{Dx} \\[2mm] d_0 = \dfrac{\rho\pi(r_{ic}^2 - r_{op}^2)DxC_p}{Dt} \\[2mm] e_0 = -2\pi r_{ip}U_p Dx \\[2mm] g_0 = -2\pi r_w DxU_a \\[2mm] F_{a(i)}^{n+1} = Q_{pl_i}^{n+1} + Q_{JT_i}^{n+1} + Q_{b_i}^{n+1} + Q_{p_i}^{n+1} \end{cases}$$

Where r_w is the open hole diameter, r_{ic} is the inner diameter of the casing, r_{op} is the outer diameter of the pipe, U_a is the overall heat transfer coefficient between the formation and the annulus.

Formation:

$$a_f T_{j,i}^{n+1} + b_f T_{j,i-1}^{n+1} + c_f T_{j,i+1}^{n+1} + d_f T_{j,i}^{n} = 0 \tag{3.7}$$

The coefficients of the **Eq (3.7)** are given as follows

$$\begin{cases} a_f = -\dfrac{2r}{Dr} + 1 - \dfrac{rDr}{\alpha Dt} \\[2mm] b_f = \dfrac{r}{Dr} - 1 \\[2mm] c_f = \dfrac{r}{Dr} \\[2mm] d_f = \dfrac{rDr}{\alpha Dt} \end{cases}$$

Where $T_{j,i}^{n+1}$ is the temperature of the formation at $x = j.Dx$, and $r = r_w + i.Dr$ at the current time.

At the wellbore wall, the discretized equation is the following

$$a_m T_{j,1}^{n+1} + c_m T_{j,2}^{n+1} + d_m T_{j,1}^n + e_m T_{a(j)}^n = 0 \qquad (3.8)$$

Where the coefficients of the **Eq (3.8)** are given as follows:

$$\begin{cases} a_m = -\dfrac{k_{for}}{Dr} - U_a - Dr.\rho_{for}.\dfrac{C_{for}}{Dt} \\[2mm] c_m = \dfrac{k_{for}}{Dr} \\[2mm] d_m = Dr.\rho_{for}.\dfrac{C_{for}}{Dt} \\[2mm] e_m = U_a \end{cases}$$

Where k_{for} is the formation thermal conductivity, C_{for} is the heat capacity of the formation, ρ_{for} is the density of the formation.

3.1.2 Matricial system

After passing from an analytical form of the equations to a an algebraical one, the temperature at every node at every moment can be found by solving a matrixial system. An equation set of $(j_{max} * (i_{max} + 2), j_{max} * (i_{max} + 2))$, shown as matrix (4.8) was found. [15]

$$\begin{bmatrix} A & H \\ P & Q \end{bmatrix}.T = B$$

Where, for $j_{max} = 4$, $i_{max} = 4$:

- *Matrix A*

$$A_{(2j_{max}*2j_{max})} = \begin{bmatrix} a & c & 0 & 0 & e & 0 & 0 & 0 \\ b & a & c & 0 & 0 & e & 0 & 0 \\ 0 & b & a & c & 0 & 0 & e & 0 \\ 0 & 0 & b & a & 0 & 0 & 0 & e \\ e_0 & 0 & 0 & 0 & a_0 & c_0 & 0 & 0 \\ 0 & e_0 & 0 & 0 & b_0 & a_0 & c_0 & 0 \\ 0 & 0 & e_0 & 0 & 0 & b & a_0 & c_0 \\ 0 & 0 & 0 & e_0 & 0 & 0 & b_0 & a_0 \end{bmatrix}$$

The implementation of the matrix A is done as shown in **Fig 6**.

```
A_0=zeros(j_max);
A_1=zeros(j_max);

E_0=zeros(j_max);
E_1=zeros(j_max);

for j=2:j_max-1
    A_0(j,j)=a(j);A_0(j,j-1)=b(j) ; A_0(j,j+1)=c(j);
    E_0(j,j)=e(j);

    A_1(j,j)=a_0(j);A_1(j,j-1)=b_0(j) ; A_1(j,j+1)=c_0(j);
    E_1(j,j)=e_0(j);
end
%Boundaries of the matrix :
A_0(1,1)=a(1); A_0(1,2)=c(1);
A_0(j_max,j_max)=a(j_max); A_0(j_max,j_max-1)=b(j_max);
A_1(1,1)=a_0(1); A_0(1,2)=c_0(1);
A_0(j_max,j_max)=a_0(j_max); A_0(j_max,j_max-1)=b_0(j_max);

E_0(1,1)=e(1) ;
E_0(j_max,j_max)= e(j_max);
E_1(1,1)=e_0(1) ;
E_0(j_max,j_max)= e_0(j_max);

A=[A_0 E_0 ; E_1 A_1];
```

Figure 5.*MATLAB code for implementing matrix* A

- *Matrix H*

$H_{2j_{max}*(2j_{max}*i_{max})}$

$$
= \begin{bmatrix}
0 & 0 & 0 & 0 & 0 & 0 & 0 & 0 & 0 & 0 & 0 & 0 & 0 & 0 & 0 & 0 & 0 & 0 & 0 & 0 \\
0 & 0 & 0 & 0 & 0 & 0 & 0 & 0 & 0 & 0 & 0 & 0 & 0 & 0 & 0 & 0 & 0 & 0 & 0 & 0 \\
0 & 0 & 0 & 0 & 0 & 0 & 0 & 0 & 0 & 0 & 0 & 0 & 0 & 0 & 0 & 0 & 0 & 0 & 0 & 0 \\
0 & 0 & 0 & 0 & 0 & 0 & 0 & 0 & 0 & 0 & 0 & 0 & 0 & 0 & 0 & 0 & 0 & 0 & 0 & 0 \\
g_0 & 0 & 0 & 0 & g_0 & 0 & 0 & 0 & g_0 & 0 & 0 & 0 & g_0 & 0 & 0 & 0 & g_0 & 0 & 0 & 0 \\
0 & 0 & 0 & 0 & 0 & 0 & 0 & 0 & 0 & 0 & 0 & 0 & 0 & 0 & 0 & 0 & 0 & 0 & 0 & 0 \\
0 & 0 & 0 & 0 & 0 & 0 & 0 & 0 & 0 & 0 & 0 & 0 & 0 & 0 & 0 & 0 & 0 & 0 & 0 & 0 \\
0 & 0 & 0 & 0 & 0 & 0 & 0 & 0 & 0 & 0 & 0 & 0 & 0 & 0 & 0 & 0 & 0 & 0 & 0 & 0 \\
0 & 0 & 0 & 0 & 0 & 0 & 0 & 0 & 0 & 0 & 0 & 0 & 0 & 0 & 0 & 0 & 0 & 0 & 0 & 0 \\
\end{bmatrix}
$$

The implementation of matrix H is done as shown in **Fig 7** :

```
for j=1:j_max
    a_H(j)=-2*ID_oh(j)*0.0254*0.5*pi*Dx(j)*U_a(j,1);
end

H=zeros(j_max,j_max*i_max);

for j=1:j_max
H(j,(j-1)*i_max+1)=a_H(j);
end
```

Figure 6. *MATLAB code for implementing matrix H*

- *Matrix P*

$$P_{(j_{max}*i_{max},2\,j_{max})} = \begin{bmatrix} 0 & 0 & 0 & 0 & e_m & 0 & 0 & 0 \\ 0 & 0 & 0 & 0 & 0 & 0 & 0 & 0 \\ 0 & 0 & 0 & 0 & 0 & 0 & 0 & 0 \\ 0 & 0 & 0 & 0 & 0 & 0 & 0 & 0 \\ 0 & 0 & 0 & 0 & 0 & 0 & 0 & 0 \\ 0 & 0 & 0 & 0 & 0 & e_m & 0 & 0 \\ 0 & 0 & 0 & 0 & 0 & 0 & 0 & 0 \\ 0 & 0 & 0 & 0 & 0 & 0 & 0 & 0 \\ 0 & 0 & 0 & 0 & 0 & 0 & 0 & 0 \\ 0 & 0 & 0 & 0 & 0 & 0 & 0 & 0 \\ 0 & 0 & 0 & 0 & 0 & 0 & e_m & 0 \\ 0 & 0 & 0 & 0 & 0 & 0 & 0 & 0 \\ 0 & 0 & 0 & 0 & 0 & 0 & 0 & 0 \\ 0 & 0 & 0 & 0 & 0 & 0 & 0 & 0 \\ 0 & 0 & 0 & 0 & 0 & 0 & 0 & 0 \\ 0 & 0 & 0 & 0 & 0 & 0 & 0 & e_m \end{bmatrix}$$

The implementation of the matrix P is done as shown in **Fig 8**:

```
F_1=zeros(j_max*i_max,j_max);

for j=1:j_max
a_F_1(j)=U_a(j,1);
end

for j=1:j_max
    s=1+(j-1)*i_max;
    F_1(s,j)=a_F_1(j);

end
```

Figure 7.*MATLAB code for implementing matrix P*

- *Matrix Q*

$$Q_{(j_{max}*i_{max},j_{max}*i_{max})} = \begin{bmatrix} q & 0 & 0 & 0 \\ 0 & q & 0 & 0 \\ 0 & 0 & q & 0 \\ 0 & 0 & 0 & q \end{bmatrix} \; where \; q = \begin{bmatrix} a_m & c_m & 0 & 0 \\ b_f & a_f & c_f & 0 \\ 0 & b_f & a_f & c_f \\ 0 & 0 & b_f & a_f \end{bmatrix}$$

The implementation of matrix Q is done as shown in **Fig 9**:

50

```
for j=1:j_max
a_m(j)=-k_f(j)/(Dr(1)) - U_a(j,1) - Dr(1)*1000*rhof(j)*c_f(j)/Dt*abc;
c_m(j)=k_f(j)/Dr(1);
d_m(j)=Dr(1)*1000*rhof(j)*c_f(j)/Dt*abc;
e_m(j)=U_a(j,1);

end
a_f1=[]; b_f1=[]; c_f1=[]; d_f1=[];

for j=1:j_max
for s=1:i_max
a_f1(j,s)= -2*r(s)/Dr(s) + 1 - r(s)*Dr(s)/(aa(j)*Dt)*abc;
b_f1(j,s)=r(s)/Dr(s) - 1;
c_f1(j,s)=r(s)/Dr(s) ;
d_f1(j,s)=r(s)*Dr(s)/(aa(j)*Dt)*abc;
end
end
F_2=zeros(j_max*i_max);
for j=1:j_max
    F_20=zeros(i_max);
for s=2:i_max-1
    F_20(s,s)=a_f1(j,s);
    F_20(s,s-1)=b_f1(j,s);
    F_20(s,s+1)=c_f1(j,s);
end
```

Figure 8.*MATLAB code for implementing matrix Q*

- *Global matrix GM*

The implementation of the global matrix and the boundary conditions are done as shown in **Fig 10**:

```
%GLOBAL MATRIX:

GM=[A,[zeros(j_max,j_max*i_max);H];[zeros(j_max*i_max,j_max),F_1,F_2]];

%Boundary conditions:
GM(1,:)=0;GM(1,1)=1;
GM(j_max,:)=0 ; GM(j_max,j_max)=1; GM(j_max,2*j_max)=-1;
GM(2*j_max,:)=0 ; GM(2*j_max,j_max) = 1;GM(2*j_max,j_max-1)=-1;
```

Figure 9.*MATLAB code for the implementation of the global matrix*

- *Vector B*

$$B_{j_{max}(2+i_{max})} = \begin{bmatrix} B_p \\ B_a \\ B_f \end{bmatrix}$$

Where

$$B_p = \begin{bmatrix} F_{p(1)}^{n+1} - d.T_{p(1)}^n \\ ... \\ F_{p(j_{max})}^{n+1} - dT_{p(j_{max})}^n \end{bmatrix}, B_a = \begin{bmatrix} F_{a(1)}^{n+1} - d_0 T_{a(1)}^n \\ ... \\ F_{a(j_{max})}^{n+1} - d_0.T_{a(j_{max})}^n \end{bmatrix}, B_f = \begin{bmatrix} -d_f T_{1,1}^n \\ ... \\ -d_f T_{j_{max},i_{max}}^n - c_f T_{geothermal(j_{max})} \end{bmatrix}$$

With
$$B_f((j-1).i_{max} + i_{max}) = -d_f T_{(j-1).i_{max}+i_{max},i_{max}}^n - c_f T_{geothermal(j)}$$

The implementation of the vector B is shown in **Fig 11**:

```
%Vector (B)

% Initilazing vectors B_0, B_1, B_2:

B_0=zeros(j_max,1);
 B_1=zeros(j_max,1);
B_2=zeros(j_max*i_max,1);

%Determining vectors B_0, B_1, B_2:

for j=1:j_max  %j_max-1
    %Pipe:       ( B_0 )
  B_0(j)= F_i(j)-d(j)*T_0(j);

    %Annulus    ( B_1 )
  B_1(j)=F_a(j) - d_0(j)*T1_0(j) ;

%Formation :   ( B_2 )

for s=2:i_max-1
    B_2((j-1)*i_max+s)= -d_f1(j,s)*Tf0((j-1)*i_max+s);
end
```

Figure 10.MATLAB code for implementing of vector B

- ***Vector T(Temperature)***

$$T = \begin{bmatrix} Tp \\ Ta \\ Tf \end{bmatrix}$$

Where

$$T_{p(j_{max})} = \begin{bmatrix} T_{p(1)}^{n+1} \\ ... \\ T_{p(j_{max})}^{n+1} \end{bmatrix}, \quad T_{a(j_{max})} = \begin{bmatrix} T_{a(1)}^{n+1} \\ ... \\ T_{a(j_{max})}^{n+1} \end{bmatrix}, T_{f(j_{max}*i_{max})} = \begin{bmatrix} T_{1,1}^{n+1} \\ T_{1,2}^{n+1} \\ ... \\ ... \\ T_{j_{max},i_{max}-1}^{n+1} \\ T_{j_{max},i_{max}}^{n+1} \end{bmatrix}$$

The vector is found by solving the system *GM.T=B* . The solution using MATLAB is presented in **Fig 12** :

```
%Determining T and T1

T_t_0=mldivide(GM,B);

%T:

temp_pipe_K=T_t_0(1:j_max,1) ;

%T_0:

temp_annular_K=T_t_0(j_max+1:2*j_max);

%Tf:
Tf=T_t_0(2*j_max+1:2*j_max+i_max*j_max);
```

Figure 11.MATLAB code to solve the matrixial system

The boundary conditions should be represented in a discretized form. The following expressions summarize both the boundary and limit conditions.

- Inlet temperature: $T_{11}^{n+1} = T_{in}$
- Temperature at bottom wellbore: $T_{a(j_{max})}^{n+1} = T_{p(j_{max})}^{n+1}$
- Far field boundary: $T_{j,\infty}^{n+1} = T_{sur} + G.x$
- Initial conditions (annulus, pipe, formation) : $T_{a(j)}^0 = T_{p(j)}^0 = T_{f(j,i)}^0 = T_{sur} + G.x$

3.2 Calculation procedure

Step 1: Introducing the input data: Measured depth, wellbore geometry data, string data, formation data, fluid data.

Step 2: Introducing the initial conditions of the pipe fluid, annulus fluid and formation, radial and axial distribution of nodes.

Step 3: After determining the number of iterations needed to get the temperature after a defined time; the time loop begins, following the coming steps: (For iteration **n**).

- *Pressure* calculation is done and will be used as previous condition (**n-1**) [**P**ⁿ⁻¹]
- *Density and viscosity(n)* of the fluid using the previous temperature and pressure. (For the 1st iteration, initial conditions are used, 2nd iteration temperature and pressure found at the 1st iteration are used, etc.)
- Calculate all the *energy sources(n)* using the properties found earlier.
- Introducing the found data for the iteration number **n** inside a function allowing the calculation of the *temperature(n)*.

Step 4: Step 3 will be repeated for the number of iterations needed n_{max}.

Step 5: To calculate the temperature after a SHUT-IN, we use the properties found at n_{max} as initial conditions and repeat the steps from **3** to **4**.

3.3 Inlet mud temperature models and their discretization

Knowing the inlet temperature of the mud plays a great role in determining the temperature distribution. For this matter, 3 different models, used in real studies are presented in this chapter. The integration of these 3 models in the MATLAB code will be explained in the last paragraph.

3.3.1 Constant inlet mud temperature:

The first model, which is the most common model, is a constant inlet mud temperature. The tank contains a mud at a constant temperature. The temperature' function takes the form:

$$T_{in}(t) = T_0 \tag{3.9}$$

The implementation of the first model is done as shown in **Fig 13**:

```
if          Option==1

Inlet=Inlet_mud_temperature;
```

Figure 12.MATLAB code for implementing the first model

3.3.2 Variable inlet temperature

Constant difference between inlet and outlet mud temperatures

The second model is to take a finite difference between the inlet temperature of the pipe and the outlet temperature, coming from the annulus. The inlet temperature function of this model is the following:

$$T_{in}(t) = T_{out}(t) - \Delta T_0 \tag{3.10}$$

Where $T_{out}(t)$ is the outlet temperature, ΔT_0 is the temperature difference between the inlet and the outlet.

The implementation of the second model is shown in **Fig 13** :

```
elseif    Option==2

Inlet=temp_annular_C(1)-Delta_temp;
```

Figure 13.MATLAB code for implementing the second model

Free convection with ambient air

The fluid exiting the wellbore and entering the tank is at a temperature higher than the average value. Adding this hotter fluid gradually raises the tank fluid temperature with time. In other words, the wellbore acts as a heat exchanger supplying heat to the tank from the formation. However, as the tank temperature increases so does the heat loss from it to the surrounding air. The tank temperature finally approaches a steady value when the heat gained from the circulating fluid (from the formation) equals the heat lost to the ambient air.
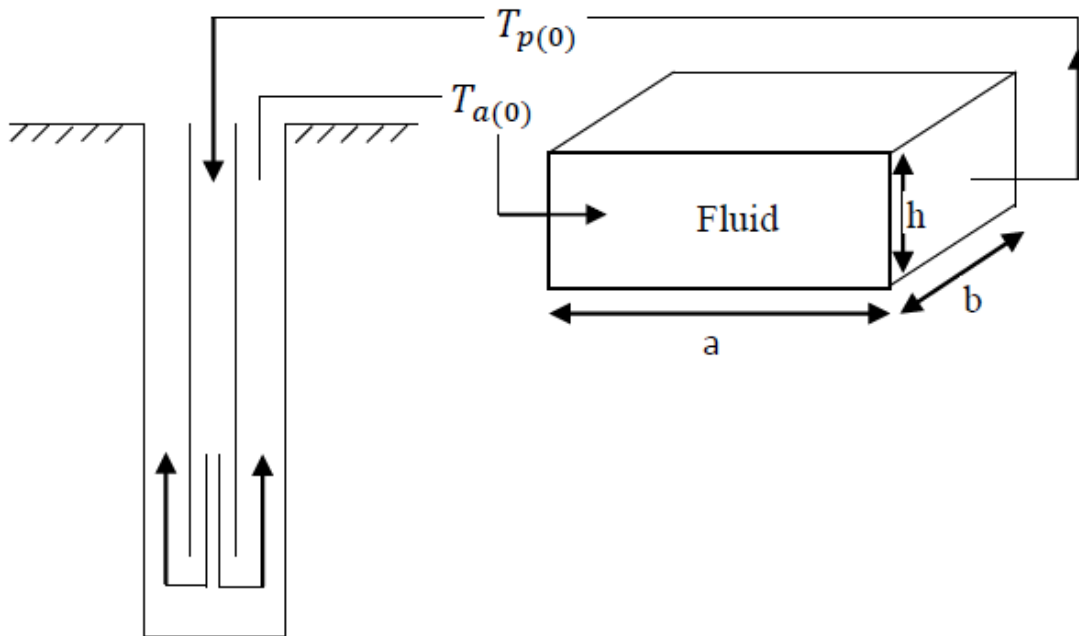
Figure 14- Schematic representation of the heat transfer model

Consider the case of forward circulation through a rectangular tank, as shown in **Fig 14**. The energy is added to the tank by the fluid entering the tank at a temperature (0) (annulus fluid exit temperature), the energy is lost from the tank by the fluid exiting the tank (and entering the wellbore) at a temperature $T_{p(0)}$, and the heat is also lost from the tank to the ambient air.

The transient energy balance for the tank is given by [7]:

$$\dot{m}C_p\left(T_{a_0} - T_{p_0}\right) + Uab\left(T_{p_0} - T_{air}\right) = \rho(abh)C_p\frac{\partial T_{p_0}}{\partial t} \tag{3.11}$$

$$\frac{\partial T_{p_0}}{\partial t} + A T_{p_0} = B \tag{3.12}$$

$$A = \frac{\dot{m} + \left(\frac{Uab}{C_p}\right)}{abh\rho} \tag{3.13}$$

$$B = \frac{\dot{m} T_{a_0} + (Uab T_{air}/C_p)}{abh\rho} \tag{3.14}$$

The solution of the **Eq (3.12)** is:

$$T_{p_0}(t) = \frac{B}{A} + Ce^{-At} \tag{3.14}$$

The coefficient C is found using the limit condition at *t=0*:

$$T_{p_0}(t = 0) = T_0$$

To find the solution of the **Eq (3.12)** , we assumed that the outlet temperature $T_{a_0}(t)$ is constant with time. This assumption comes from the fact that the outlet temperature has small variations with time. Even more, the term $m T_{a_0}$ is much smaller than the term $Uab T_{air}/C_p$.

Calculation of U

U in this case is equal to h the CHTC and considering the case of a forced convection in an external flow with a flat plate we can calculate h using correlations from [8].

To determine CHTC, the physical properties of the air are needed. Being in contact with the mud, the air temperature changes; so does its properties. It is reasonable to take the air at the film temperature:

$$T = \frac{T_{air} + T_0}{2}$$

All the following properties are calculated at this temperature:[9]

$$\rho = \frac{351.99}{T} + \frac{344.84}{T^2} \tag{3.15}$$

$$\mu = \frac{1.4592.T^{\frac{3}{2}}}{109.1 + T} \tag{3.16}$$

$$k = \frac{2.334 * 10^{-3} * T^{\frac{3}{2}}}{164.54 + T} \tag{3.17}$$

$$C_p = 1030.5 - 0.19975.T + 3.9735.10^{-4}.T^2 \tag{3.18}$$

$$Nu = 0.664 . Re^{\frac{1}{2}} . Pr^{\frac{1}{2}} \quad for\ Pr > 0.6\ \ and\ \ Re \le 5.10^5$$

$$Nu = \left(0.037 Re^{\frac{4}{5}} - 871\right) Pr^{1/3}\ \ for\ \ Pr > 0.6\ \ and\ 5.10^5 \le Re \le 10^8$$

The implementation of the third model is shown in **Fig 15:**

```
elseif     Option==3
    T_tank=300 ; T_air =298;
    aa=1;
    bb=1;
    hh=1;
    T_m= (T_tank + T_air)/2;
    Ro = 351.99/T_m + 344.84/T_m^2;
    Mu = 1.4592*T_m^(3/2)/ ( 109.1 + T_m );
    kk = ( 2.334*10^-3*T_m^(3/2))/(164.54 + T_m );
    Cp = 1030.5 - 0.19975*T_m + 3.9735*10^-4*T_m^2 ;
    U=200;

    AA= ( EDD_i(1,3)*1000*Q/1000/60 + U*aa*bb/Cp) / (aa*bb*hh*Ro);
    BB= (Ro*aa*bb*hh*temp_annular_C(2) + (U*aa*bb*T_air/Cp)) / (aa*bb*hh*Ro);
    CC= T_tank - BB/AA;

    Inlet= AA / BB  +  CC*exp(-AA*n*Dt*abc);

end
```

Figure 15.*MATLAB code for implementing the third model*

3.4 Model validation

The model needs to be validated.

The validation is done by comparing the result of our steady model, without introducing the different energy sources, nor the effect of pressure and temperature on fluid properties.

We adopt the data set used by Kabir el al(1996). This data is the foundation of the verification. In figure (4.2), the temperature of the inside pipe fluid and annulus are compared with the results of Kabir el al (1996).
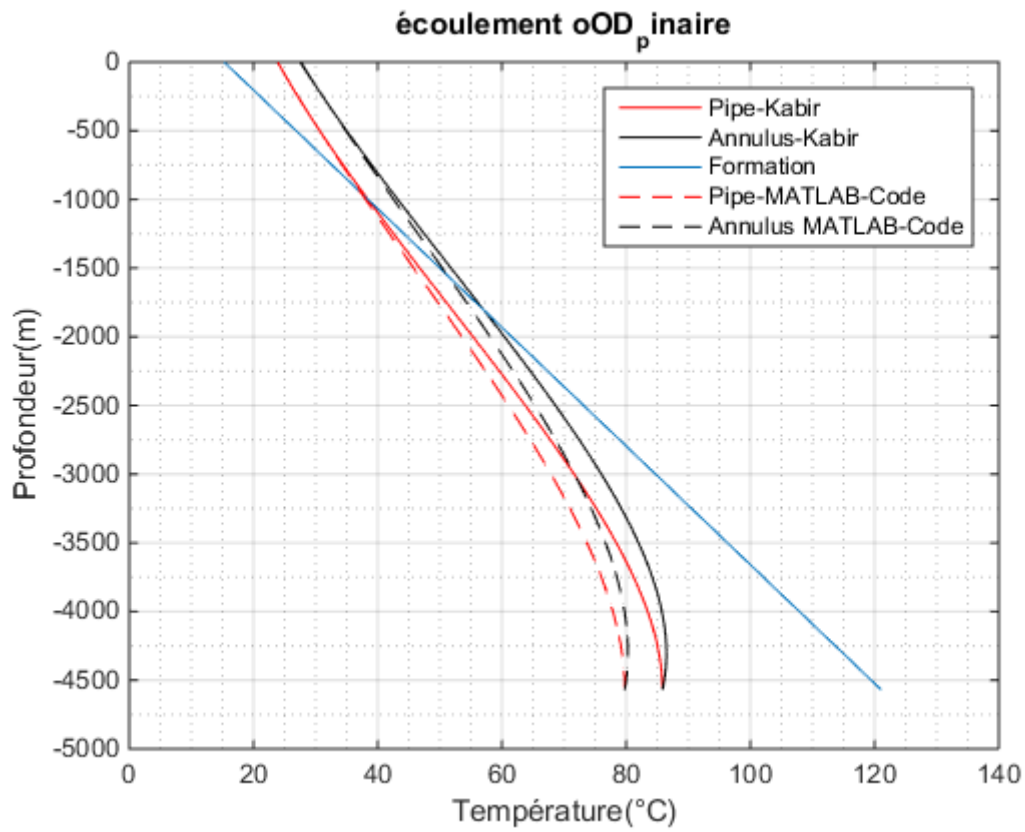
***Figure 16**.Model validation (1) with Kabir et al (1996) data*

As shown in **Fig 16**, the model presented in this study coincides with the Model presented by Kabir et al for a measured depth inferior to 2000m. Going deeper, the temperature distribution begins to slightly diverge from the values obtained by Kabir. At the bottom hole, a difference of 5^0 is observed which is reasonably acceptable.

Chapter 4: Results and discussion

Introduction

In this section, a sensitivity analysis of the developed temperature model is presented with respect to drilling operations. The objective is to determine to what extent a set of parameters of the temperature model will impact the temperature distribution. For the analysis of a given parameter, all the other parameters of the base case (Table 4.1) remain constant. We will start by investigation the flow rate; then other parameters are investigated such as drilling fluid properties. The simulations are performed for a circulation time of **5 hours**.

First, input used for this analysis is shown in the following table:

Wellbore data	
Measured depth(m)	5000
Open hole outer diameter(in)	8.5
Casing outer diameter(in)	13
Casing inner diameter(in)	12
Casing thermal conductivity(W/m.K)	45.17
Casing heat capacity(J/k.Kg)	460.5
String data	
Pipe outer dimeter(in)	5
Pipe inner diameter(in)	4.278
Pipe thermal conductivity(W/m.K)	4
Pipe heat capacity(J/Kg.K)	496
Formation data	
Formation thermal conductivity(W/m.K)	2
Formation thermal capacity(J/Kg.K)	1000
Formation density(Kg/m^3)	2500
Geothermal gradient(K/m)	0.023
Fluid data	
Fluid density(Kg/m^3)	1250
Fluid thermal conductivity(W/m.K)	0.5
Fluid heat capacity(J/Kg.K)	1430
Plastic viscosity (SI)	15
Yield point (SI)	15
Flow rate(l/min)	2000

Table 4. Wellbore data

4.1 Flow rate

One of the parameters that affects the temperature distribution is the flow rate. To investigate this impact, two distinct simulations were performed with two different values of flow rate. The results of the simulations with a flow rate of 500 l/mi, and 2000 l/min are given in **Fig 17** and **Fig 19** respectively. **Fig 18** and **Fig 20** show the variation of bottom temperature and outlet temperature with time.
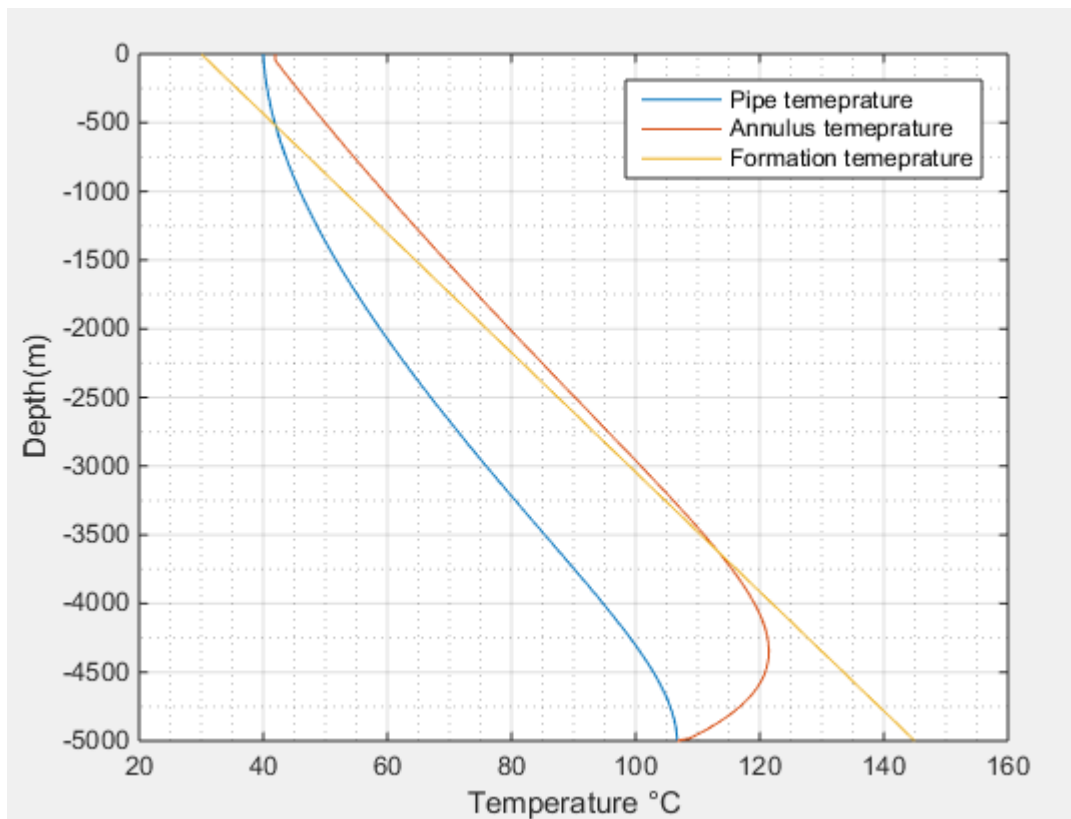
Figure 17. Temperature distribution for a flow rate of 500l/min
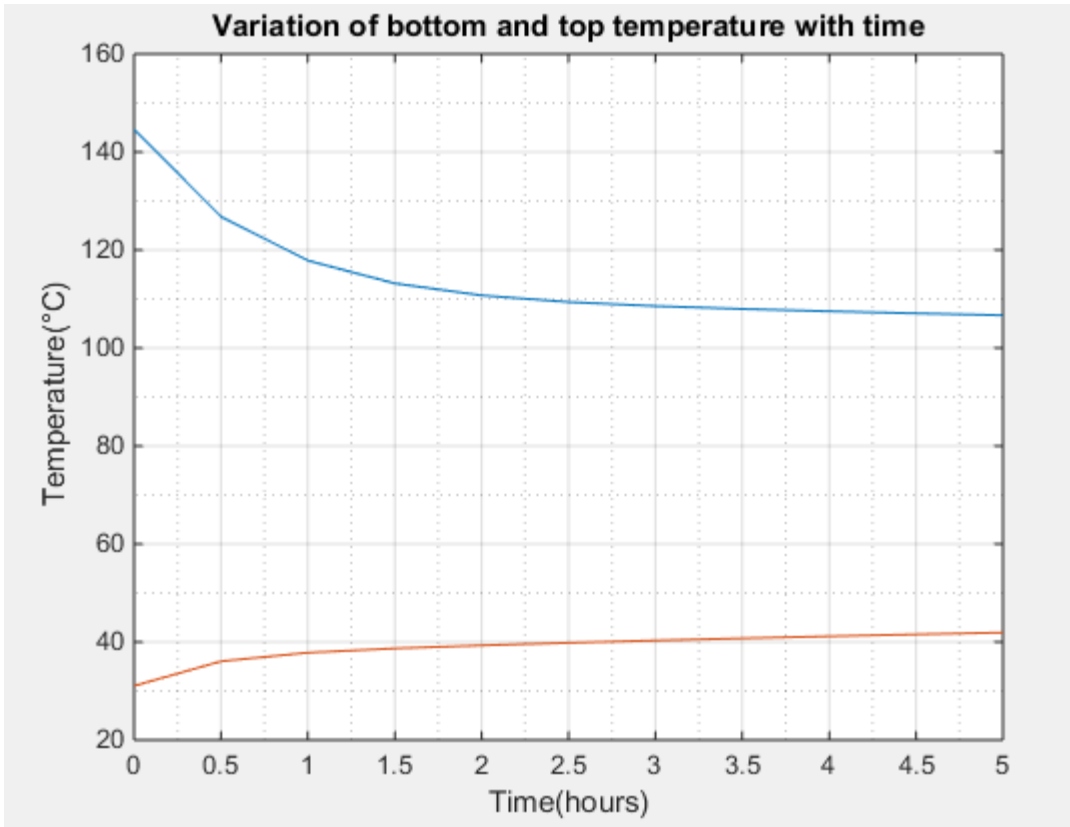
Figure 18*-Variation of bottom and outlet temperature with time (*500l/min*)*
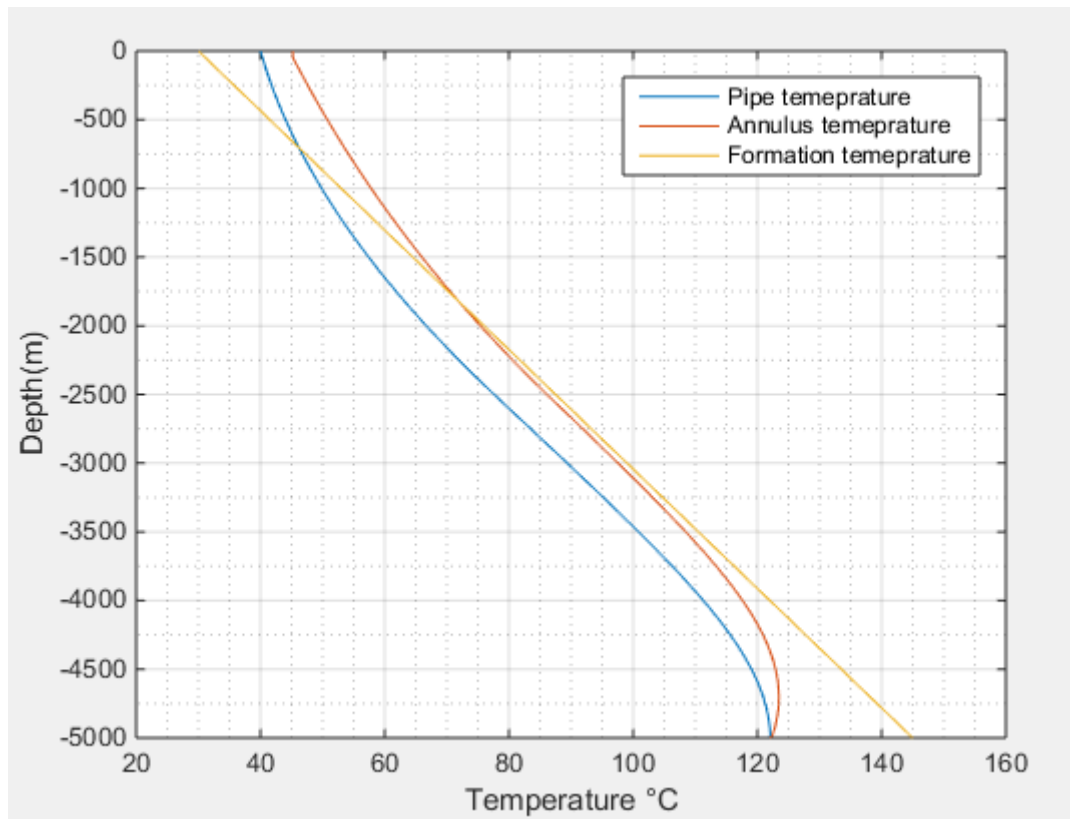
Figure 19. *Temperature distribution for a flow rate of 2000 l/min*
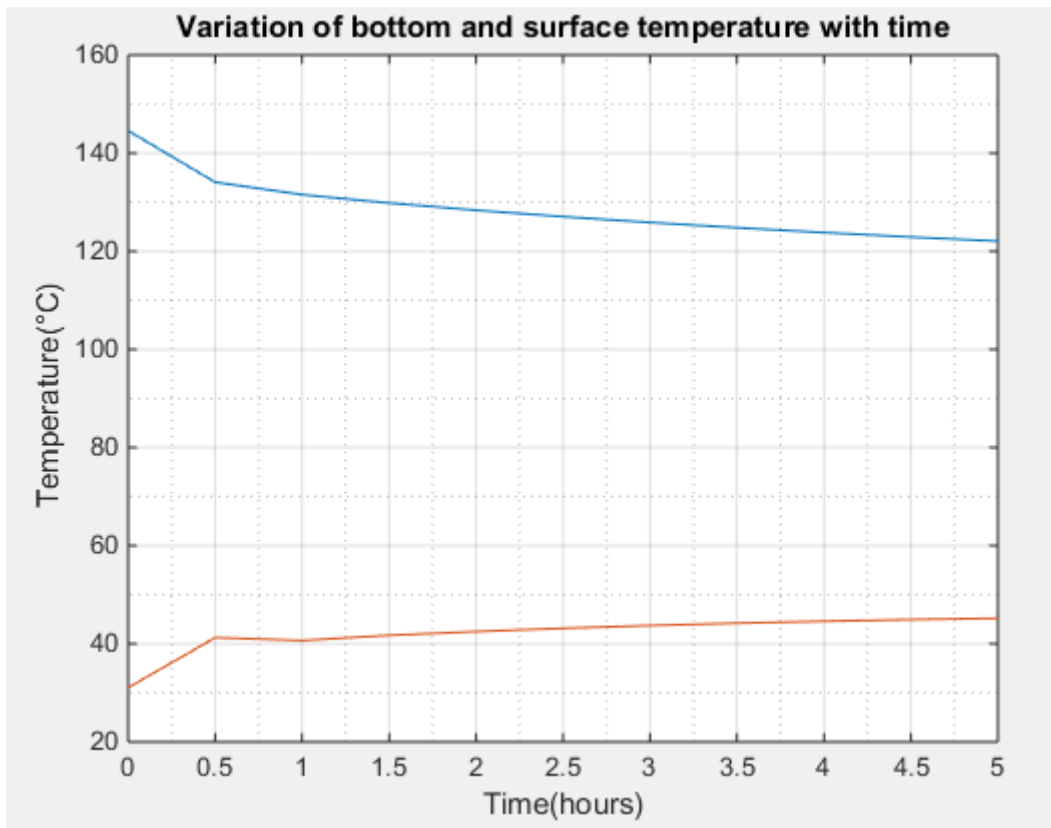
Figure 20- Variation of bottom and outlet temperature with time (2000 l/min)

Observations:

- From **Fig 17** and **Fig 19**, we notice that the temperatures changed significantly where the bottom temperature leaped from 107°C to 123°C at 5000 m of depth.
- From **Fig 18** and **Fig 20,** we notice that the bottom hole temperature decreases while the outlet temperature increases, taking constant values with time. (Converge to a steady state)

Explanations:

With increasing the flow rate, two main phenomena occur. The first one is that the flow regime changes from the laminar to the turbulent and so increasing the heat transfer coefficients $U_a \ and \ U_p$ leading to a pick in temperature, and the second one is that it will take less time for the fluid to travel from the inlet to the outlet, making the time of contact between the fluid elements small and as a consequence decreasing the energy transferred during the same time. These two parameters make the temperature of the fluid shifts from its initial condition greater when the flow rate is lower.

4.2 Specific heat capacity

The sensitivity of the mud's temperature distribution to the heat capacity of the fluid is studied in this chapter. Simulations have been performed for two different Heat capacity values. The following figures show the results obtained for the values 1430 J/Kg. K and 4000 J/Kg. K.
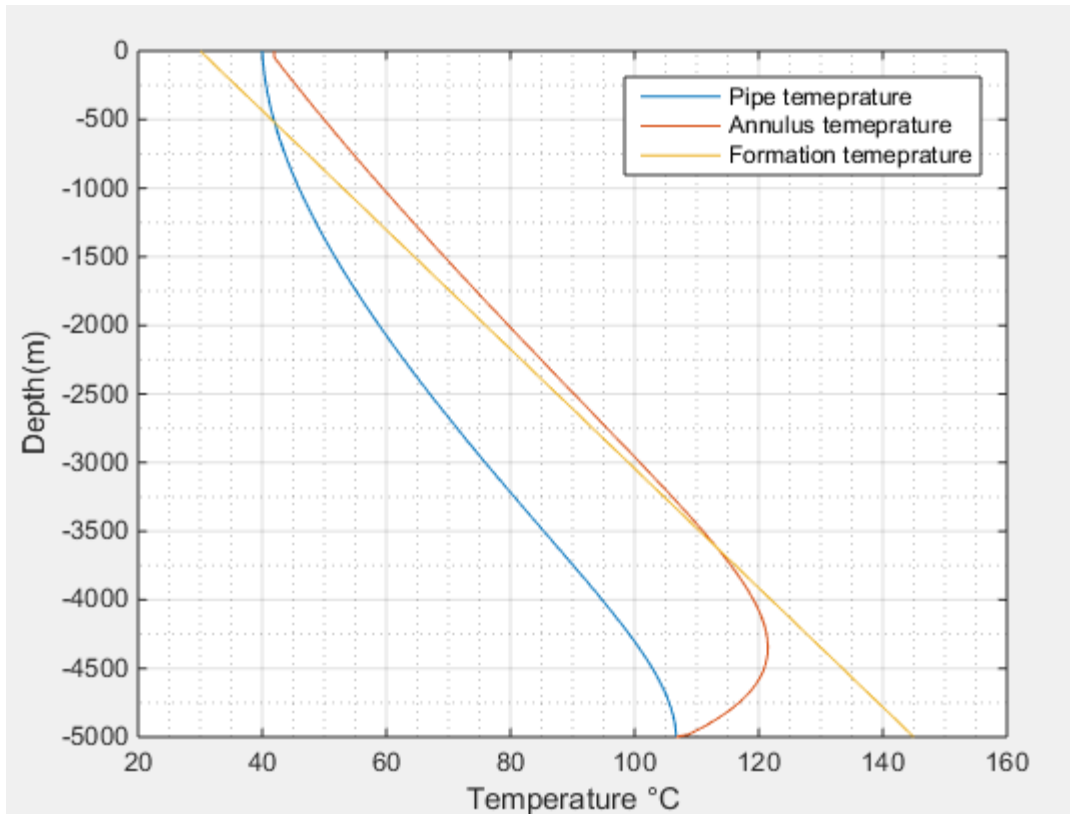
Figure 21. *Temperature distribution for a capacity of 1430 J/Kg.K*
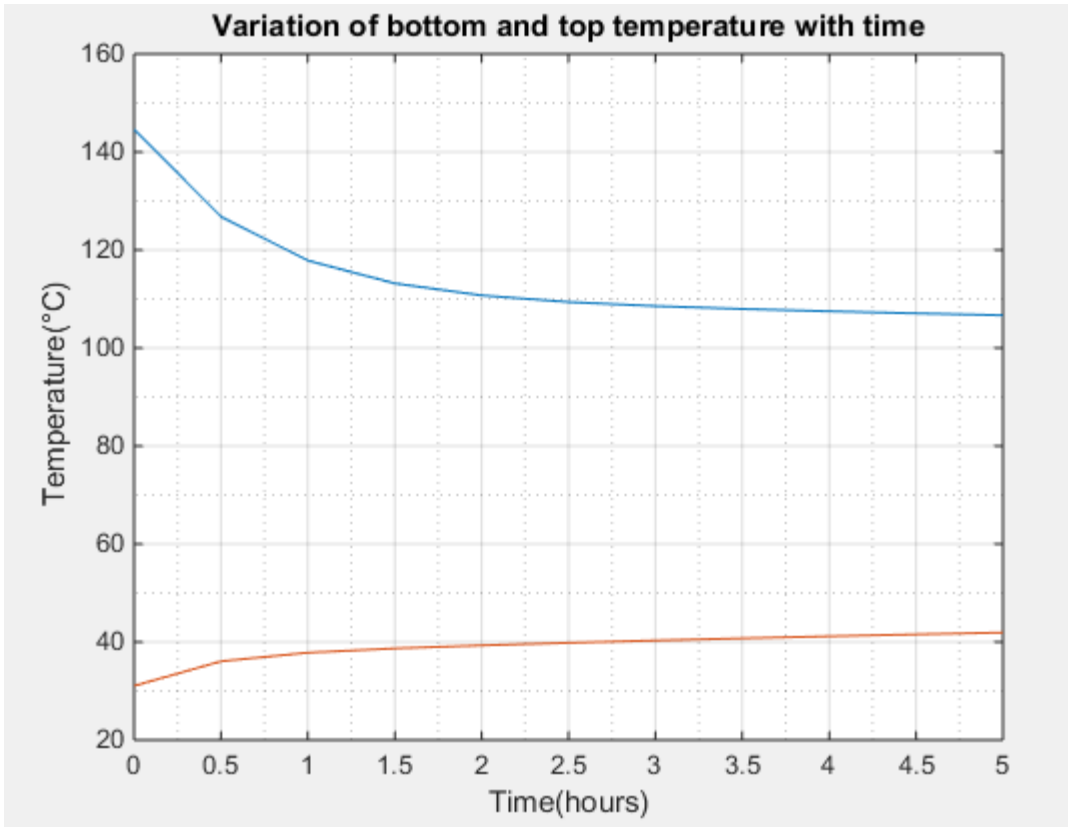
Figure 22*- Variation of bottom and outlet temperature with time (1430 J/Kg.K)*
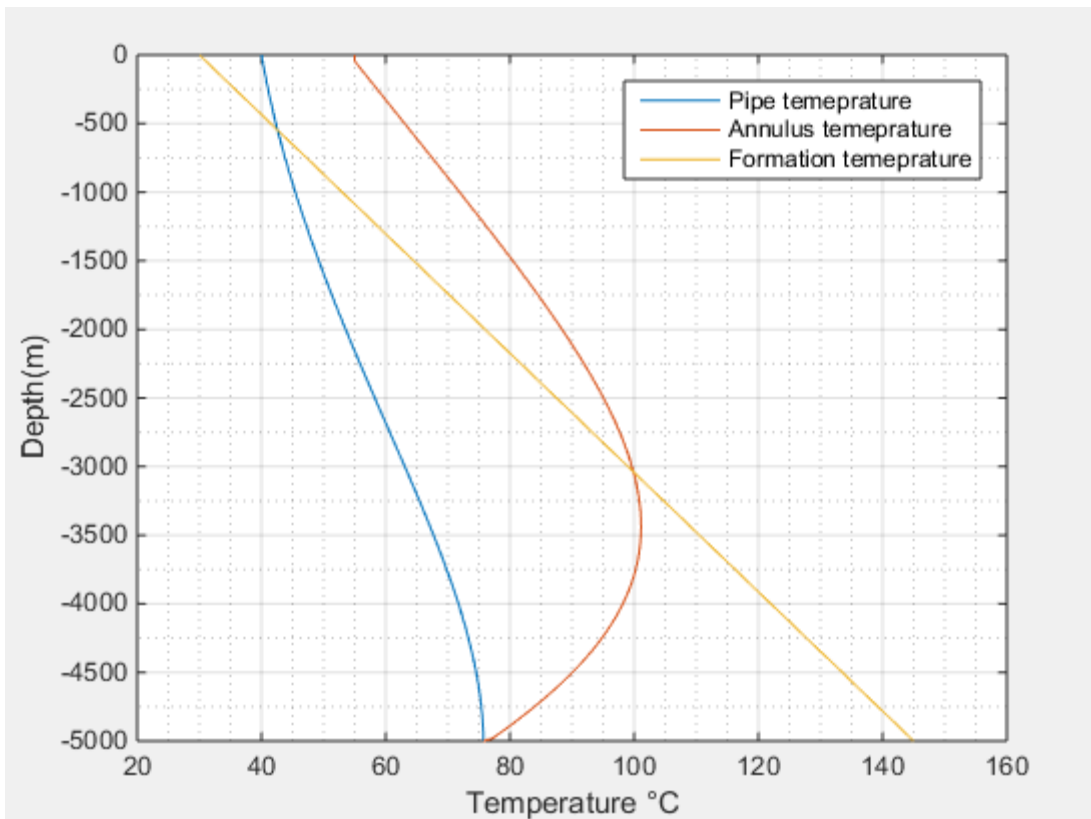
Figure 23*.Temperature distribution for a capacity of 4000 J/Kg. K*
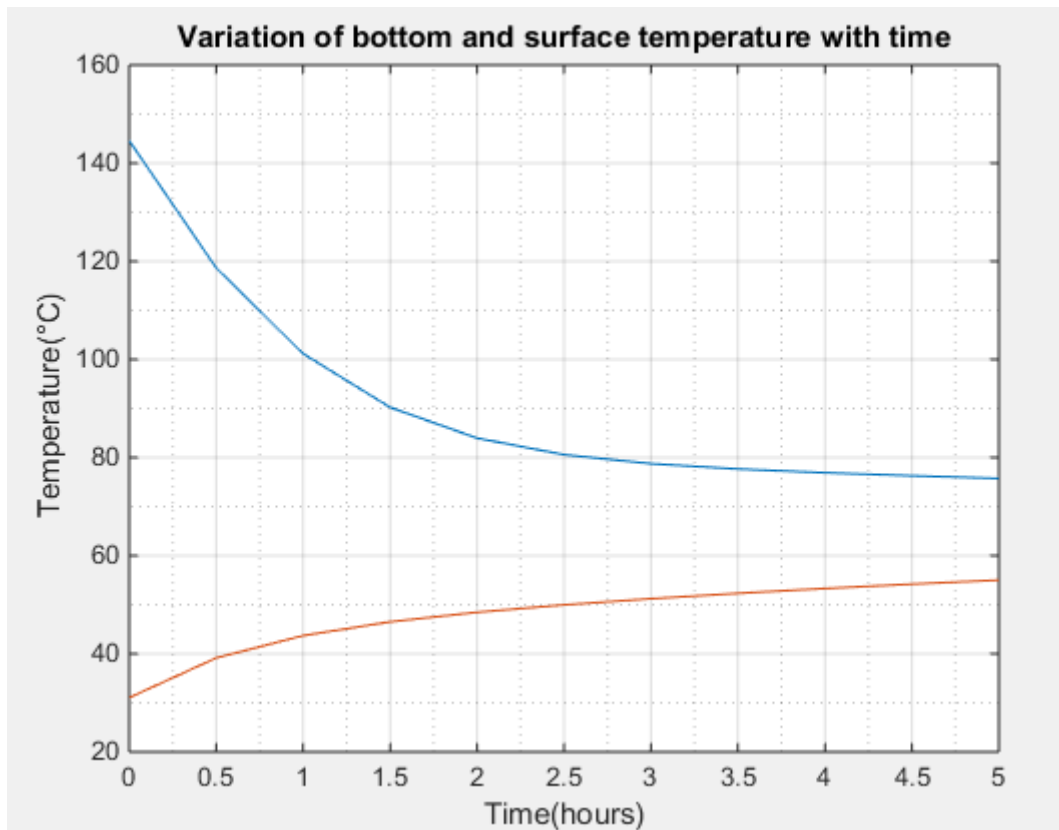
Figure 24- The variation of bottom and outlet temperature with time (4000 J/Kg. K)

Observations:

- We notice a big difference between the two curves shown in **Fig 21** and **Fig 23**. The temperature decreased globally when increasing the fluid' capacity. The bottom hole decreased by 31 °C while the outlet temperature increased by 12°C .

Explanations:

With a higher heat capacity, the fluid tends to lose energy (Decreased temperature). The mass transport is responsible for this drop. The more the heat capacity increases, the energy getting out of each cell is bigger, making it lose more energy and dropping its temperature. The entire fluid will behave exactly as one cell does.

4.3 Thermal conductivity

Fluid
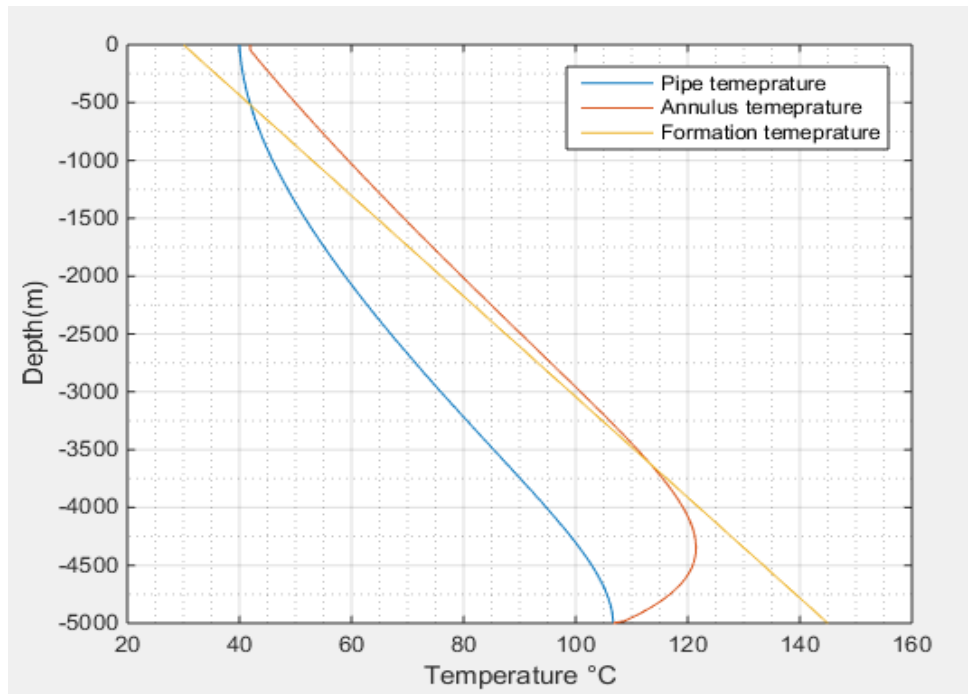
Figure 25*.Temperature distribution for a thermal conductivity of 1 W/m.K*
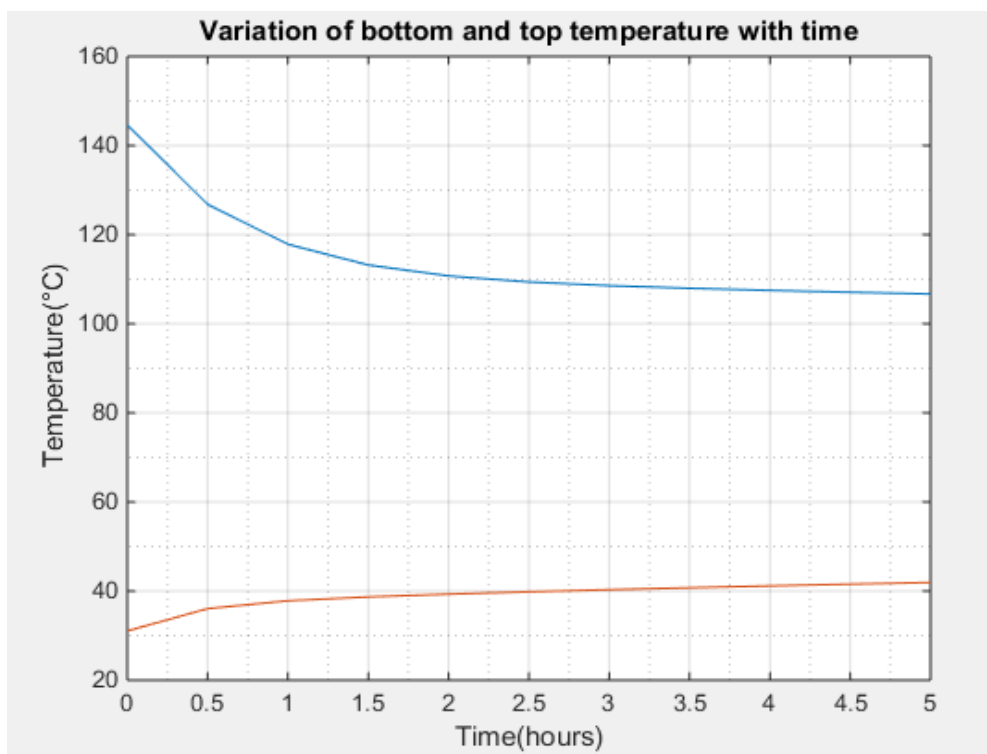
Figure 26*- Variation of bottom and outlet temperature with time (1 W/m.K)*
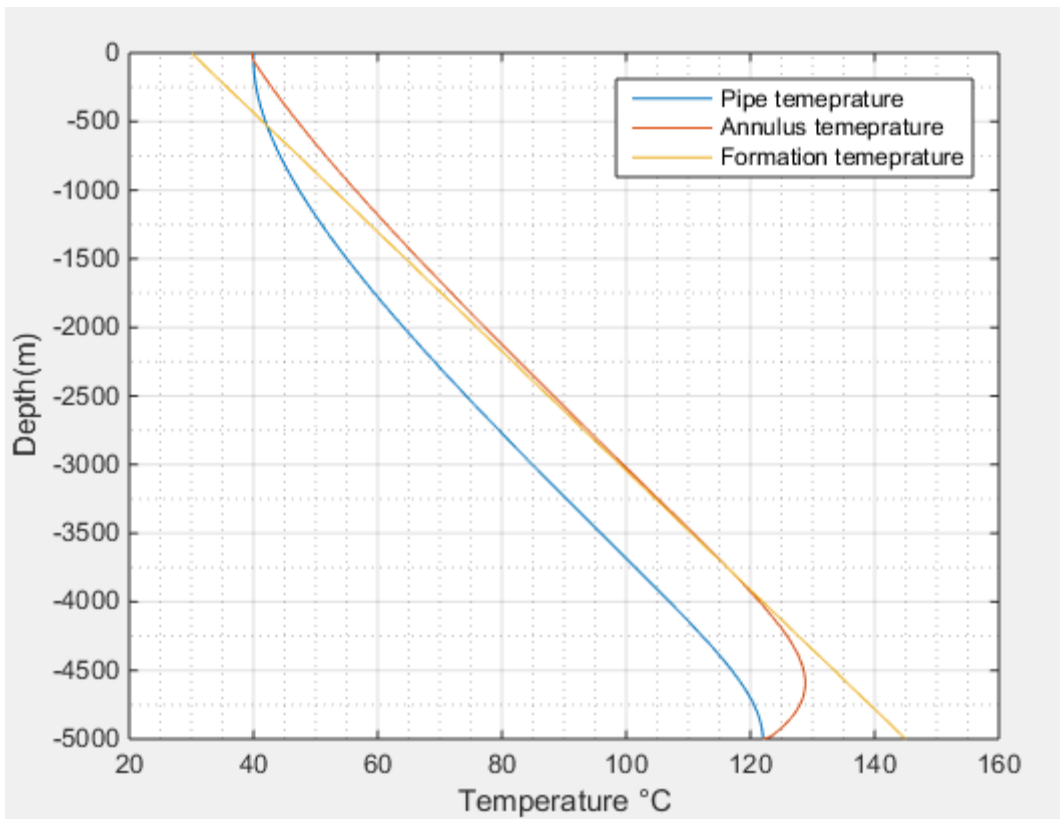
Figure 27. *Temperature distribution for a thermal conductivity of 3 W/m.K*
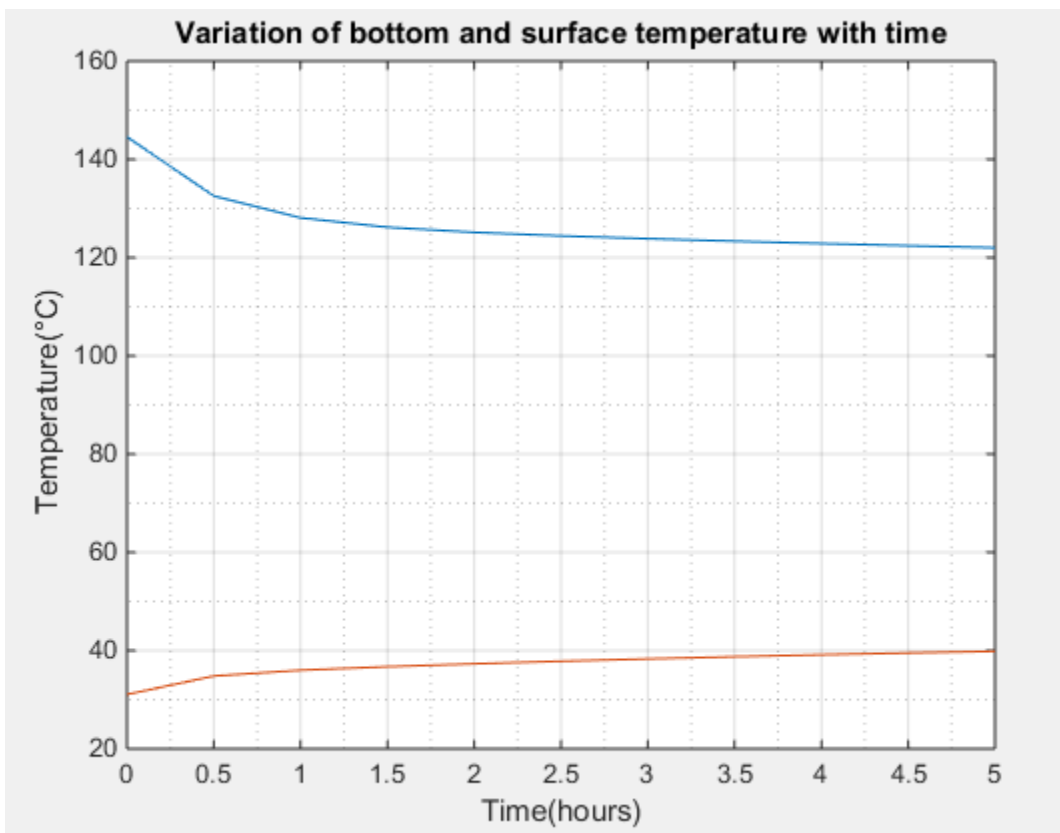
Figure 28-*Variation of bottom and outlet temperature with time(3 W/m.K)*

The impact of thermal conductivity is presented in this part. The simulations have been performed using values of thermal conductivity included in the domain: 0.5 to 3 W/m.K. For two distinct values (1 W/m.K and 3W/m.K), simulation 'results are shown in **Fig 25** and **Fig 27**. We notice that by increasing the thermal conductivity the temperature also increases. This increase is due to the heat transfer from the bottom hole node to the upper nodes. The greater the temperature of the bottom is, the more its effect on the upper nodes is noticed.

Formation

As shown in the previous chapter, formation interacts in the heat transfer and it affects the temperature distribution, it seems that varying its thermal conductivity will have consequences. **Fig 29** and **Fig 30** show the temperature distribution for two different values: 1 W/m. K and 3W/m. K respectively. For an increase in conductivity, the temperature decreases at the bottom hole by 1°.
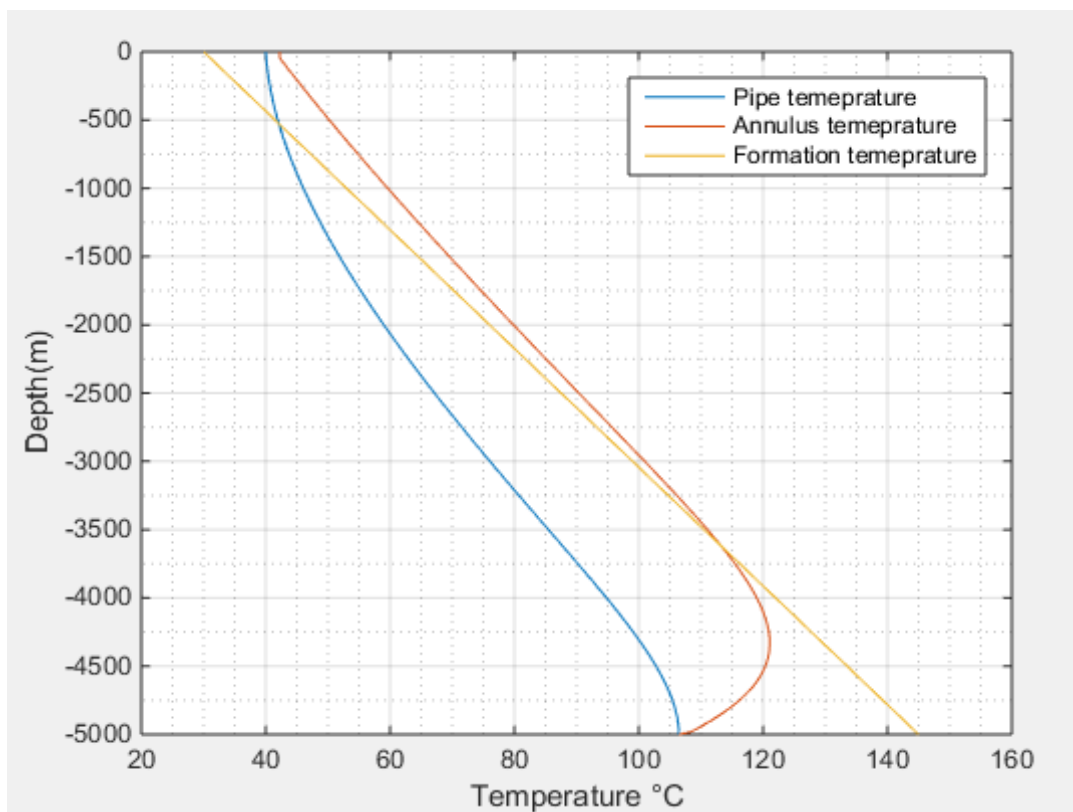
Figure 29. *Temperature distribution for a formation' thermal conductivity of 1W/m.K*
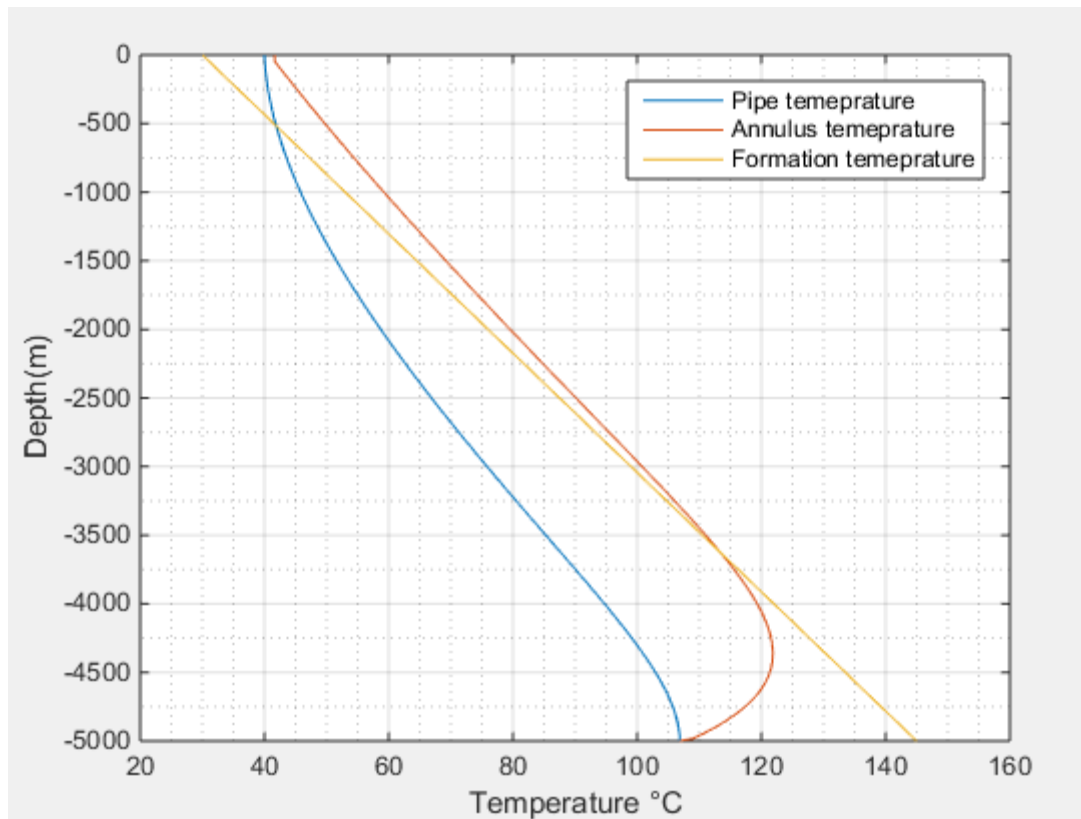
Figure 30. *Temperature distribution for formation 'thermal conductivity of 3 W/m.K*

4.4 Fluid density

The effect of density should be investigated since it intervenes in determining the heat exchange. The fluid density is responsible for the amount of heat transported during the circulation. The density of the fluid is already varying since it is affected by the pressure and temperature. The value we need to change is the density at reference conditions. To determine the effect of drilling fluid density on the temperature distribution, the reference point is varied over a range of 1000-2000 kg/m^3. **Fig 33** and **Fig 35** give the results for drilling fluids with a density of 1000 and 2000 kg/m^3 respectively.
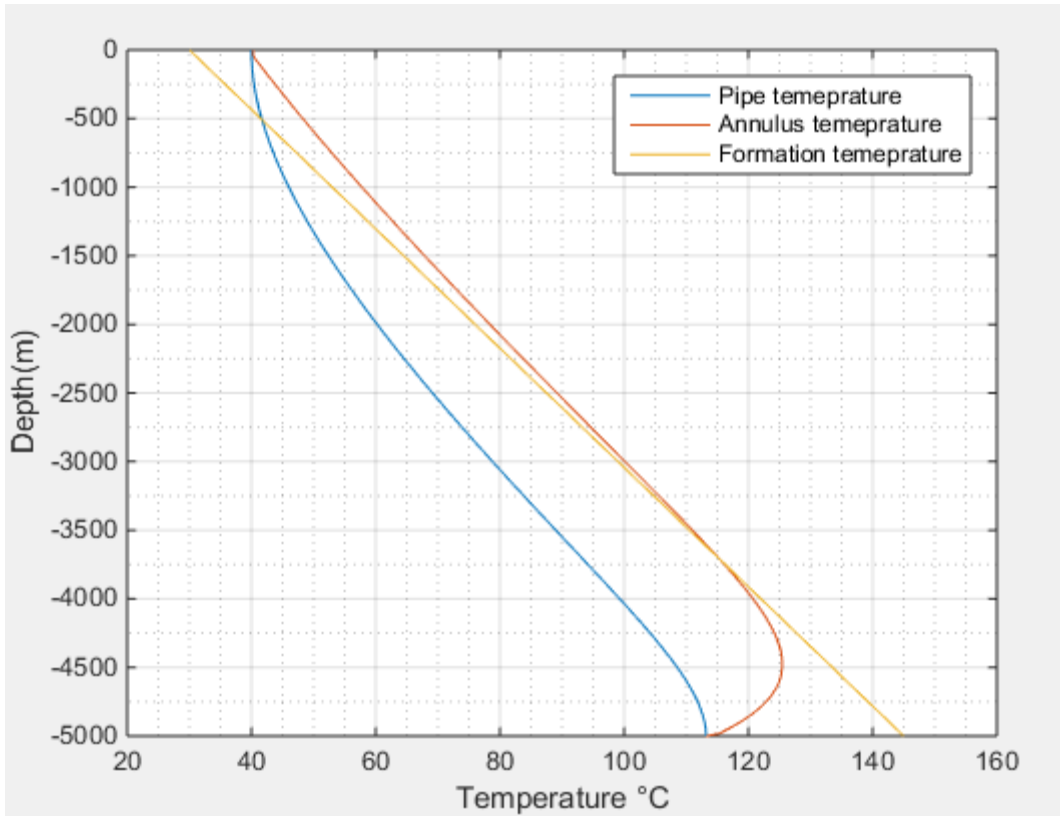
Figure 31*. Temperature distribution for a Density of 1000 Kg/m³*
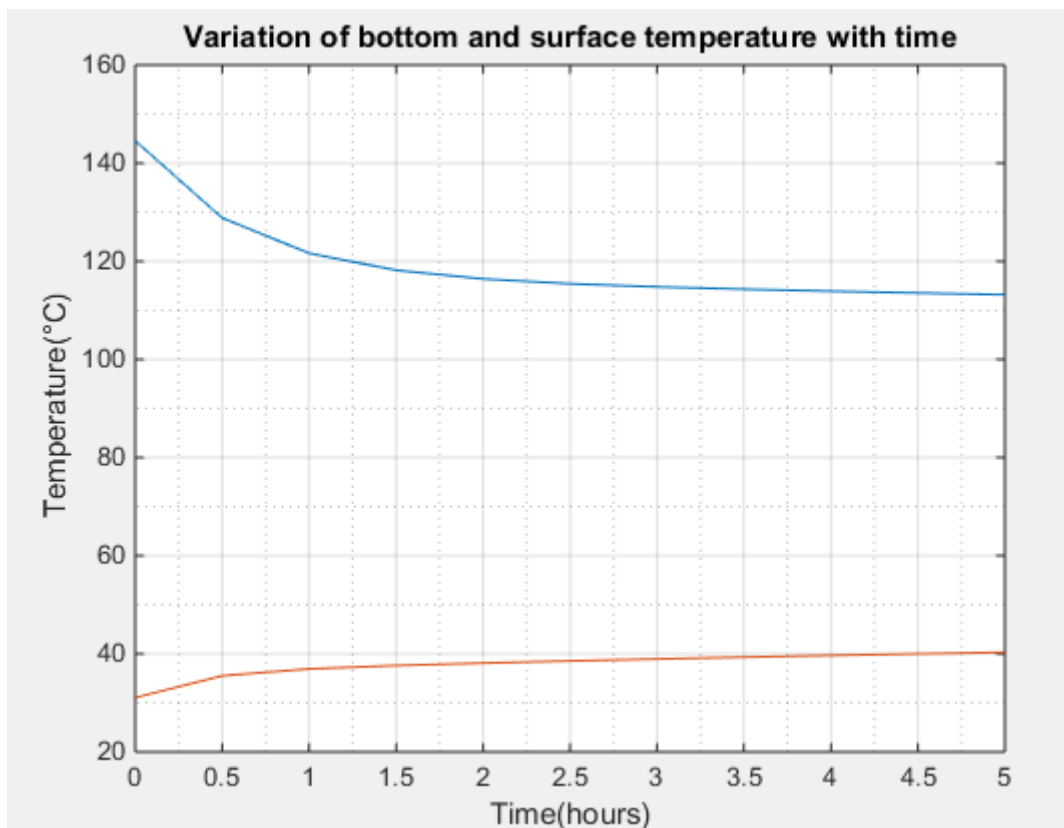
Figure 32*-Variation of bottom and outlet temperature with time(1000 Kg/m³)*
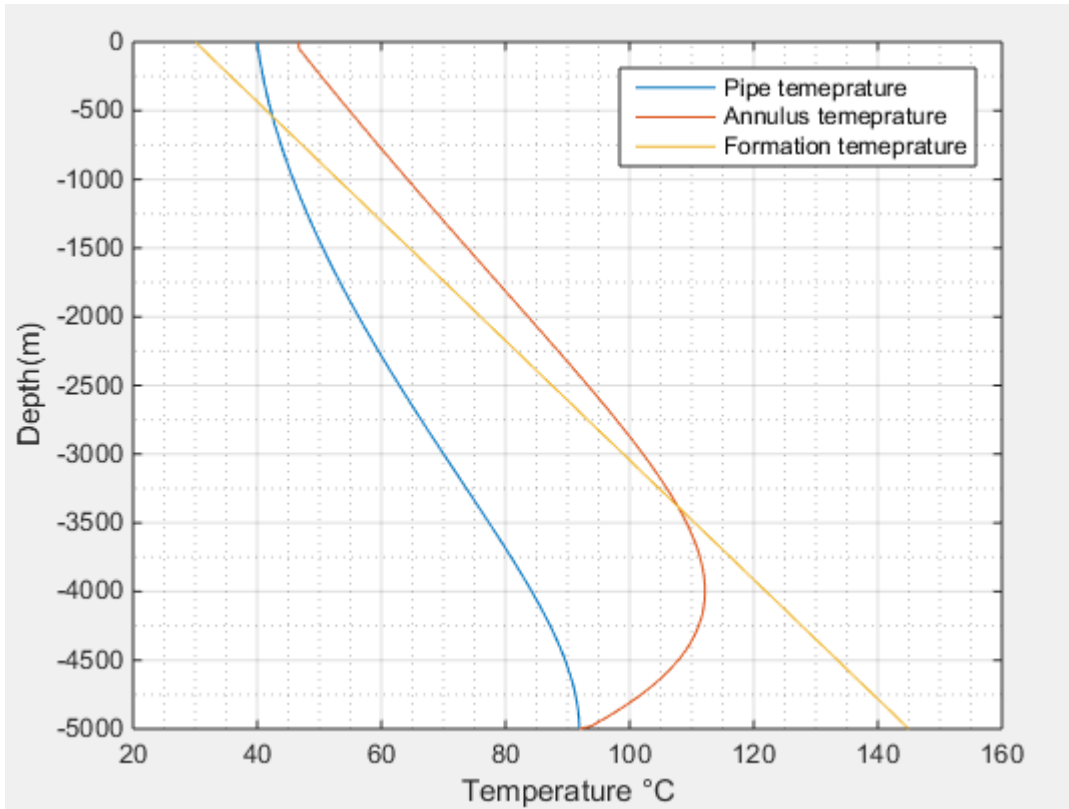
Figure 33. *Temperature distribution for a fluid Density of 2000 Kg/m³*
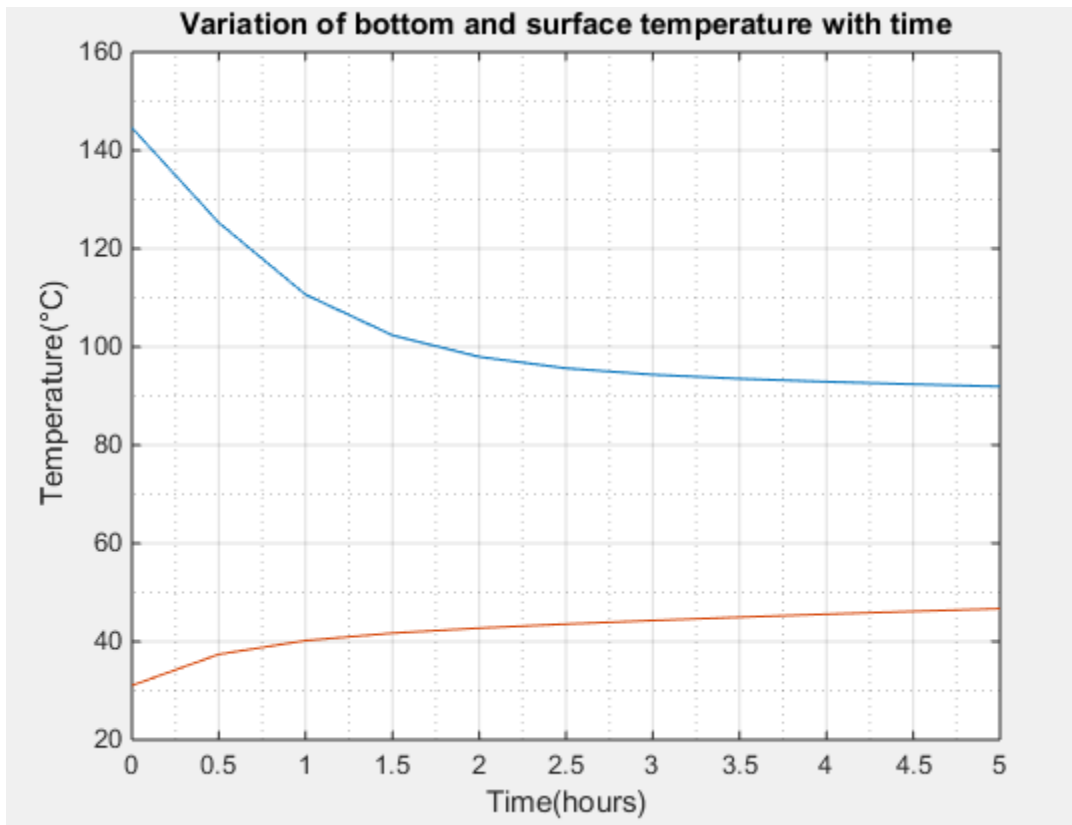
Figure 34-*Variation of bottom and outlet temperature with time (2000 Kg/m³)*

Observations:

By comparing the results obtained in the first case (1000Kg/m^3) and the second one (2000 Kg/m^3), the temperature drops from 113°C to 91 °C .

Explanation:

By increasing the density, more heat will be lost out of the wellbore resulting in a decrease of the temperature of the fluid at each depth.

4.5 Geothermal gradient
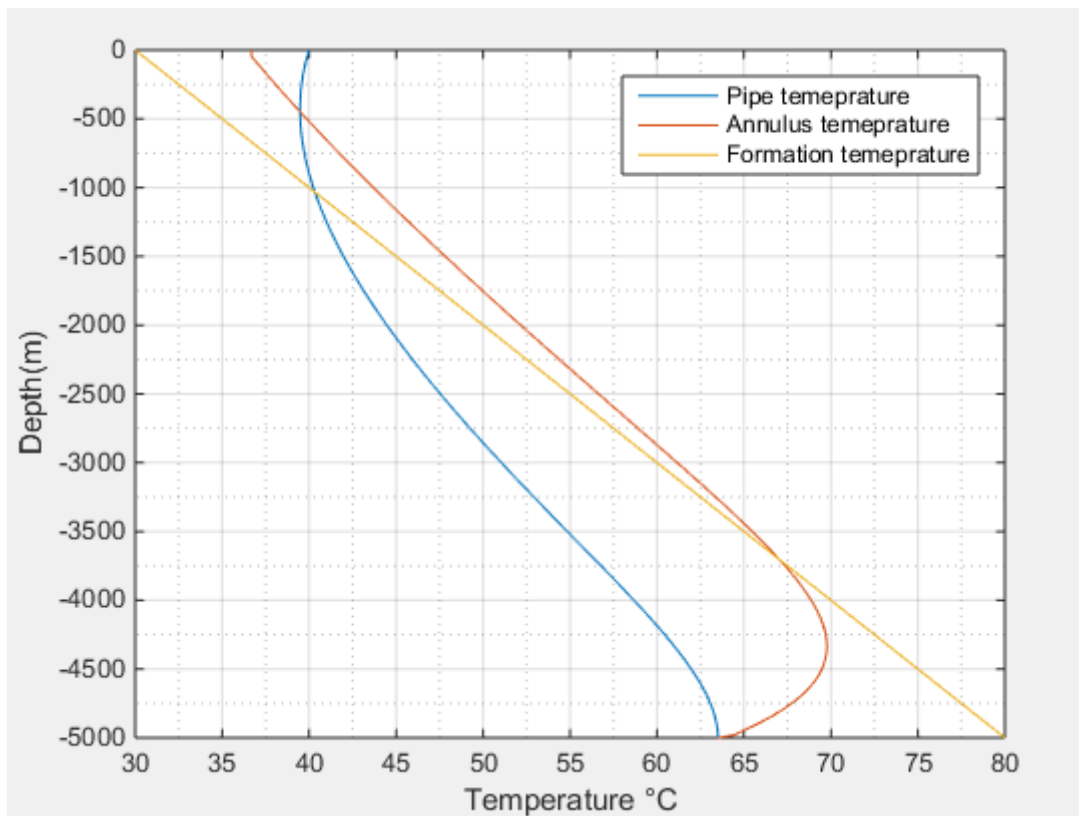
Figure 35. *Temperature distribution for a geothermal gradient of 10 K/Km*
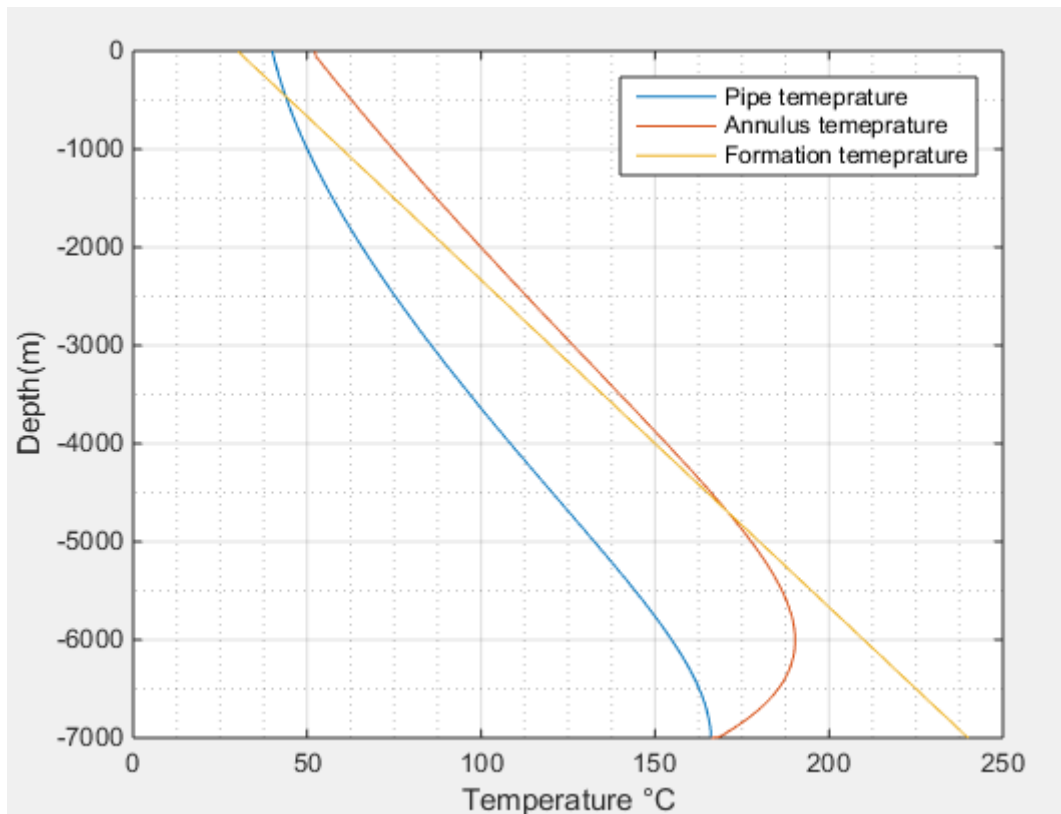
Figure 36. *Temperature distribution for a geothermal gradient of 30 K/Km*

The geothermal gradient determines the formation temperature which affects the amount of heat transferred from the formation to the annulus fluid. **Fig 35** and **Fig 36** show the difference between the temperature distribution for a gradient equal to 10 K/Km and 30 k/Km respectively.

Observations:

By increasing the geothermal gradient, a remarkable increase of temperature is observed. The bottom hole temperature leaped from 63 °C to 163 °C.

Explanations:

The formation temperature which depends on the geothermal gradient affects the fluid temperature. The energy transferred from the formation to the fluid depends on the temperature of the formation. The greater it is, the more is the energy absorbed by the fluid causing an increase in its temperature.

4.6 Mud inlet temperature model
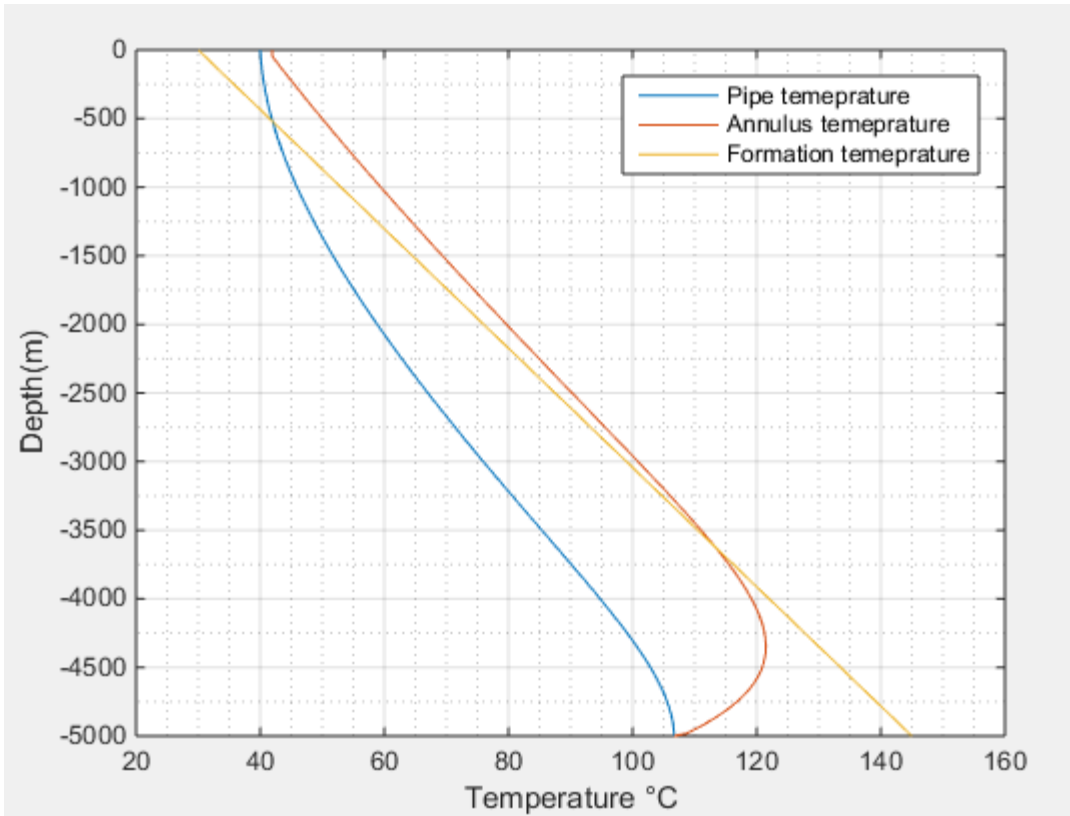
Figure 37. *Temperature distribution for a constant inlet temperature*
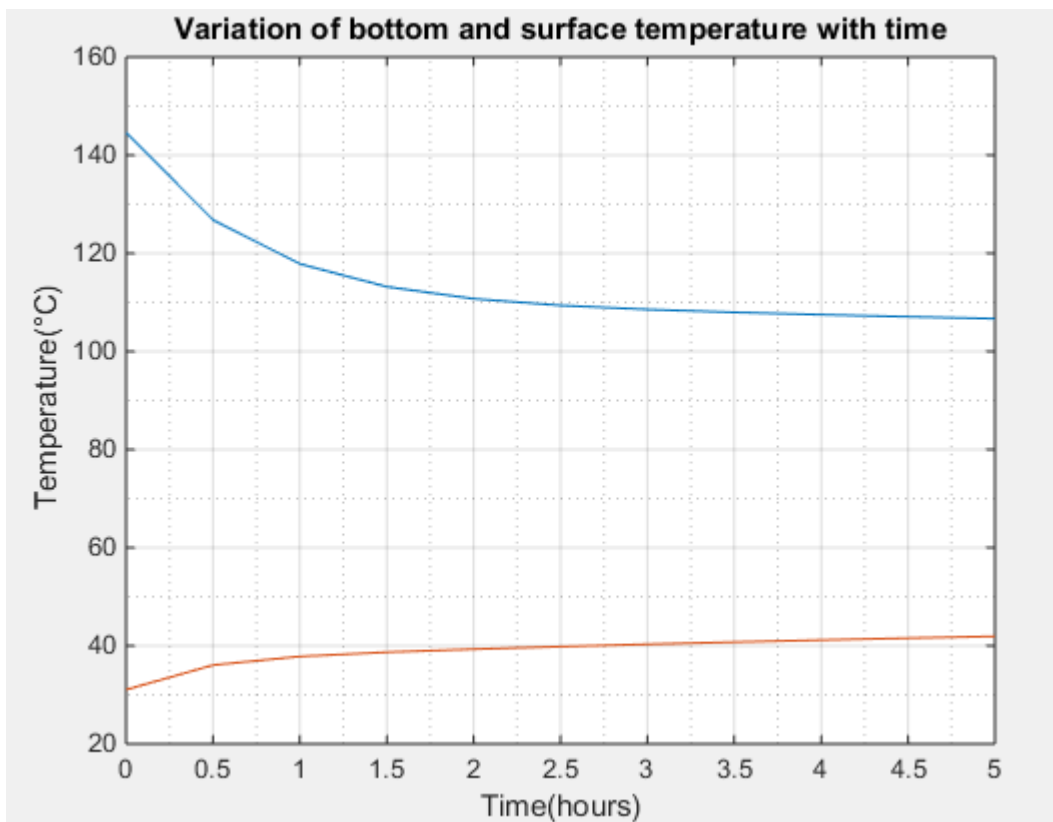
Figure 38- *Variation of bottom and outlet temperature with time (Constant inlet)*
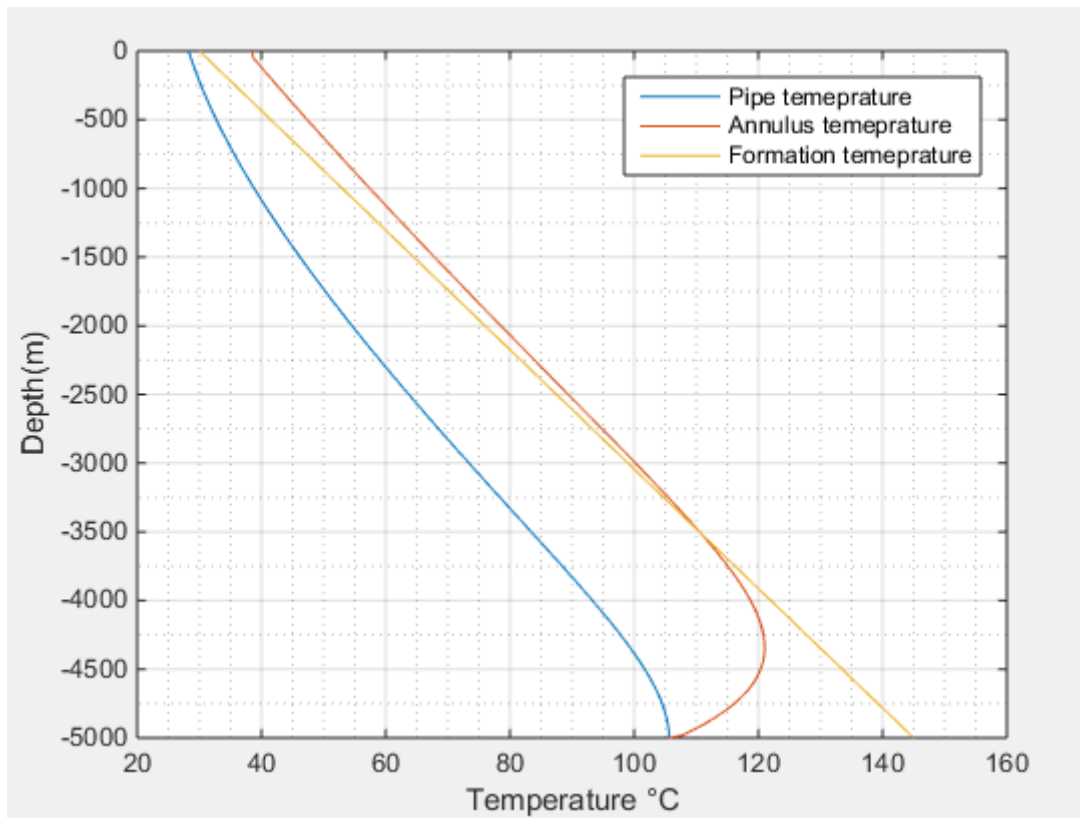
Figure 39. *Temperature distribution for a constant difference*
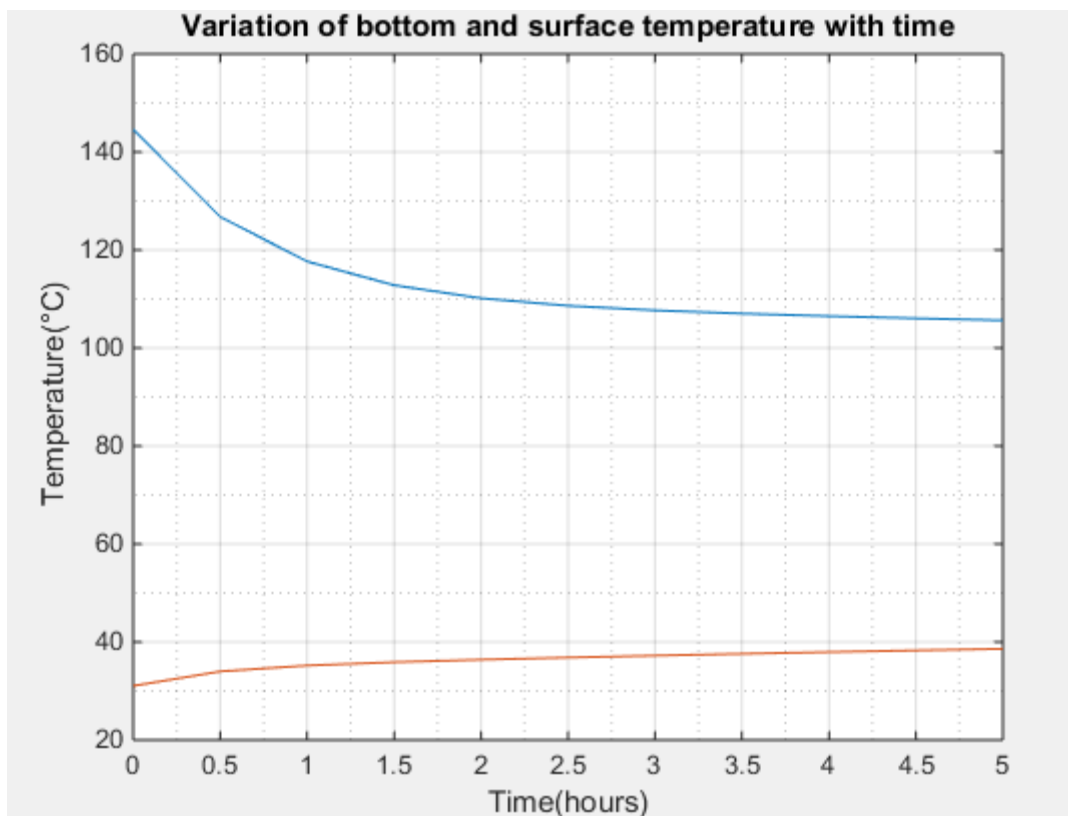
Figure 40- Variation of bottom and outlet temperature with time (Constant difference)
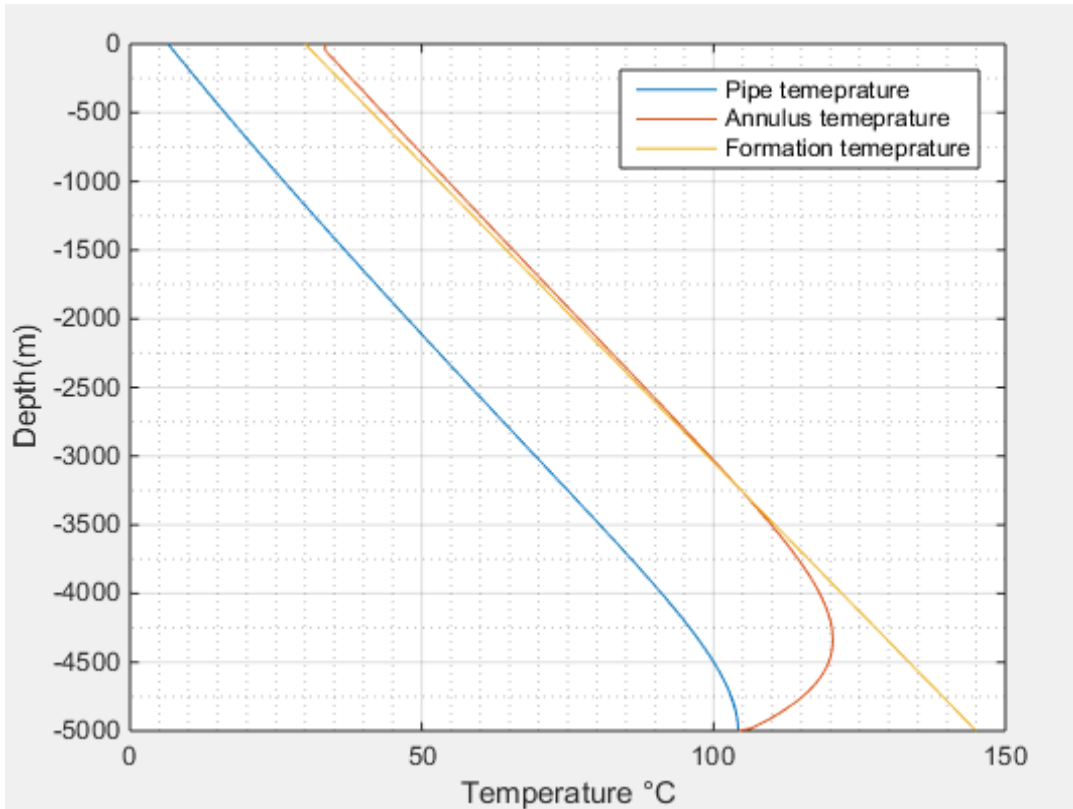
Figure 41. *Temperature distribution for a changing difference*
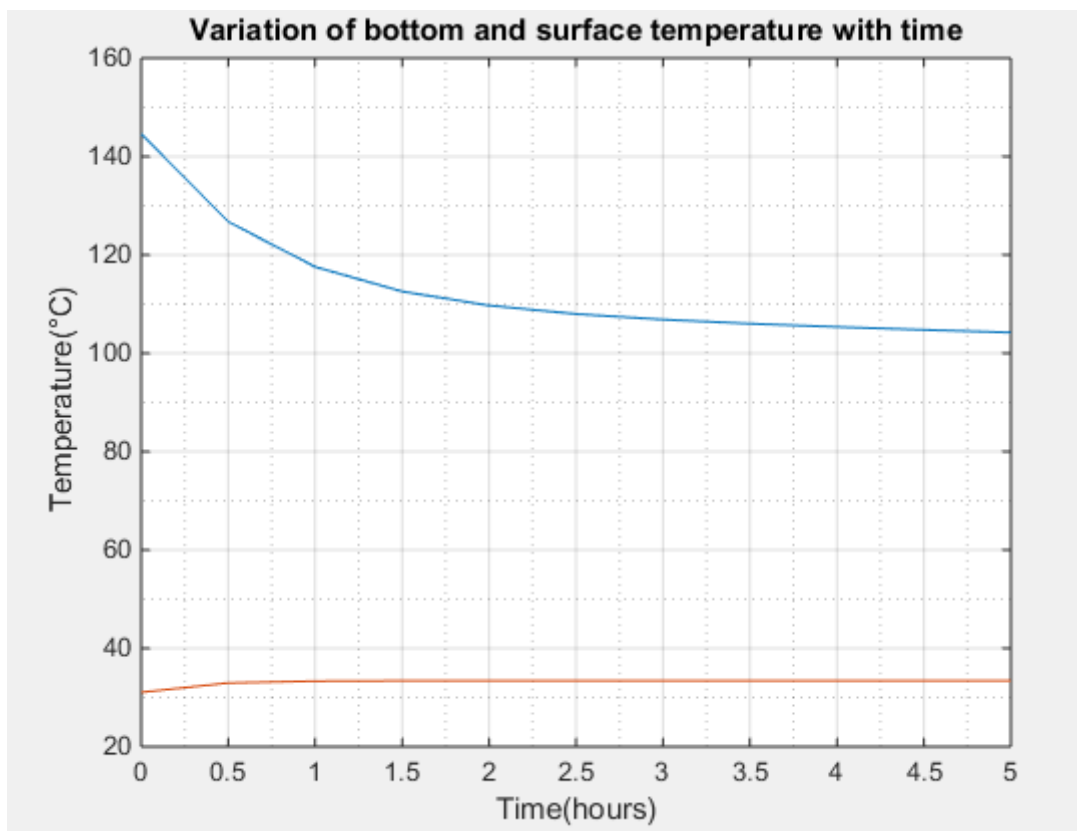
Figure 42-*Variation of bottom and outlet temperature with time (Changing difference)*

Observation

Different models have been presented in chapter 3.3. The temperature distribution varies for each model. The **Fig 37 , Fig 39, Fig 41** show the results obtained when using : constant inlet temperature, constant difference and variable difference respectively.

- For the first case (Constant inlet temperature), the mud's inlet temperature remains constant during the circulation.
- For the second case, the difference between the inlet and the outlet temperatures is constant during the circulation. Since the outlet temperature is increasing with time, the inlet temperature increases also. The temperature distribution tends to take higher values.
- For the last case, inlet temperature is calculated by introducing the cooling effect of the air on the fluid. The inlet temperature is harder to determine and it affects the temperature as shown in **Fig 41**.
- From **Fig 38**, **Fig 40** and **Fig 42**, we notice that the outlet temperature takes lower values when passing from the constant inlet model to the constant difference to the changing difference.

4.7 Effect of pressure and temperature

The variations of thermophysical properties of drilling fluids with temperature and pressure affects the wellbore temperature calculation. Studies showed that both thermal conductivity and specific heat capacity have negligible effect on the temperature distribution. The density and the viscosity are affected by the variations of pressure and temperature of the fluid and their variation should be considered to obtain an accurate temperature distribution. If the effect of the variation in viscosity and density with temperature is ignored, it will cause a large error in the calculation result of wellbore temperature distribution, especially the calculation results of wellbore temperature near the bottom-hole. [17]

Simulations have been performed for both constant and variables properties of the fluid in order to confirm or reject the assumptions stated earlier on whether the variable aspect of the fluid properties has a considerable effect on the temperature distribution or its effects can be neglected.

Fig 43 shows the results when the fluid properties are variables (Note that the function of density and viscosity with temperature are presented in chapter 2.3.1 and 2.3.3 respectively) while **Fig 44** present the temperature distribution for the same conditions except for the fluid properties which are considered constant.

Fig 45 shows the viscosity distribution inside the annulus and pipe and above it, **Fig 46**, shows the variation of density with depth.
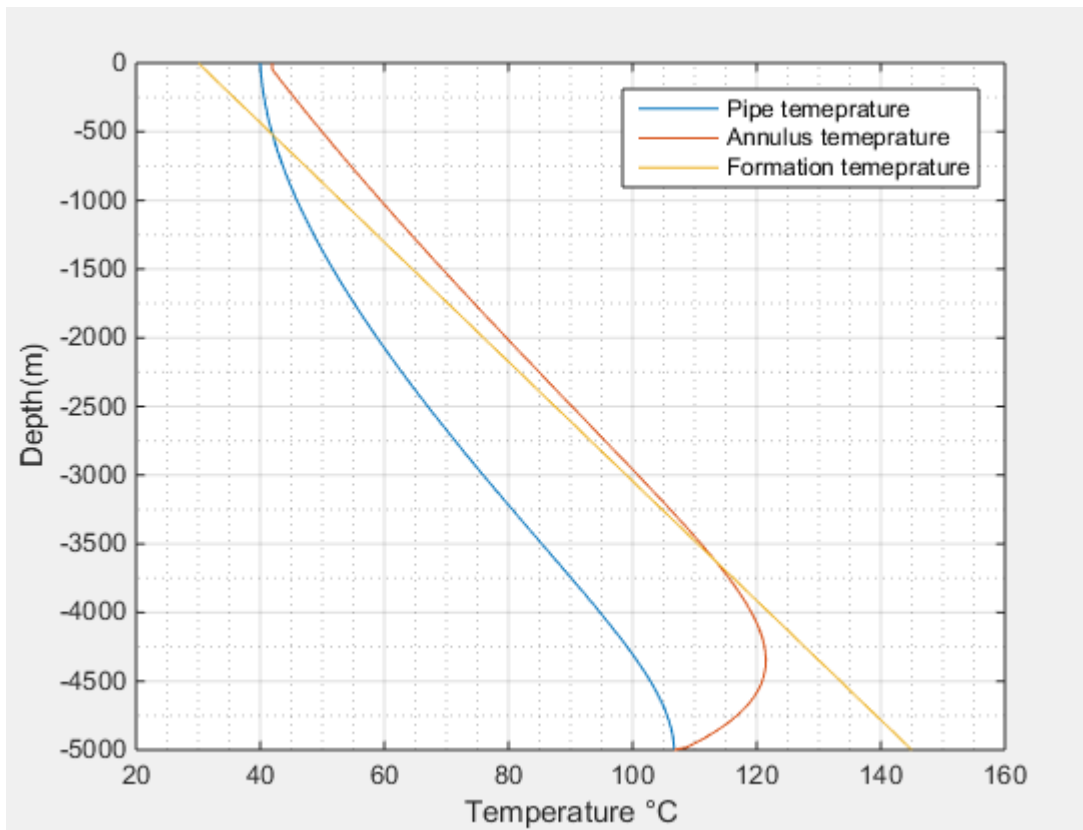
Figure 43. *Temperature distribution for variable fluid properties*
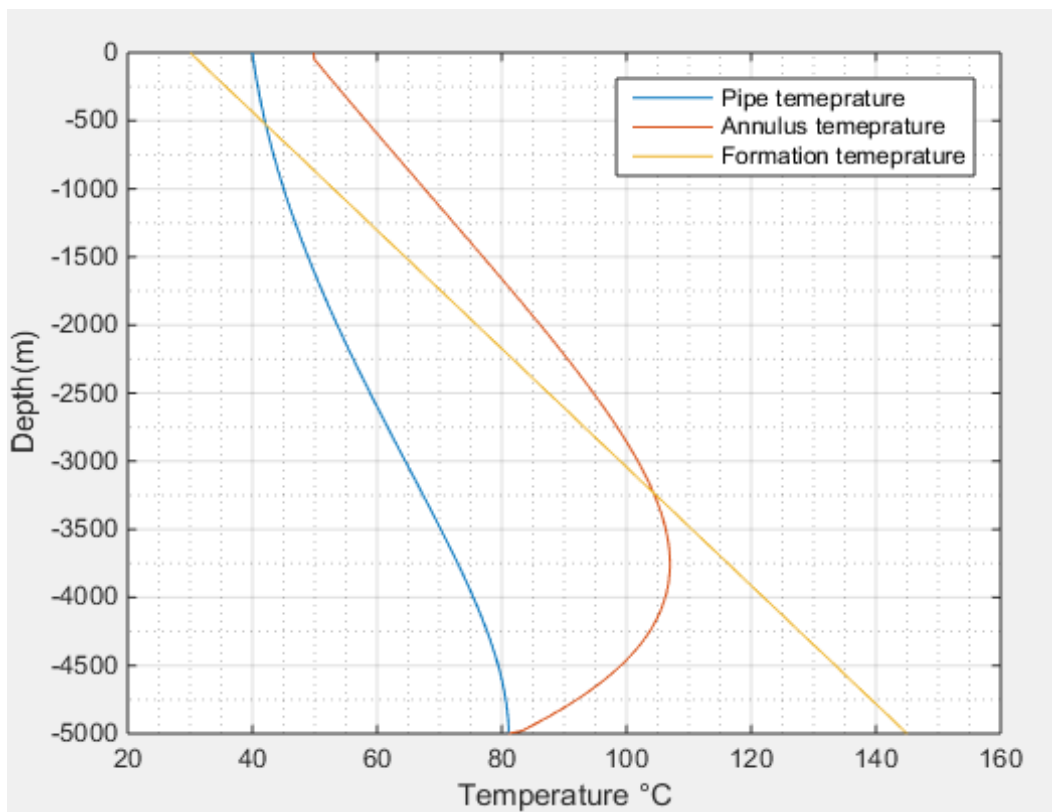
Figure 44. *Temperature distribution for constant fluid properties*
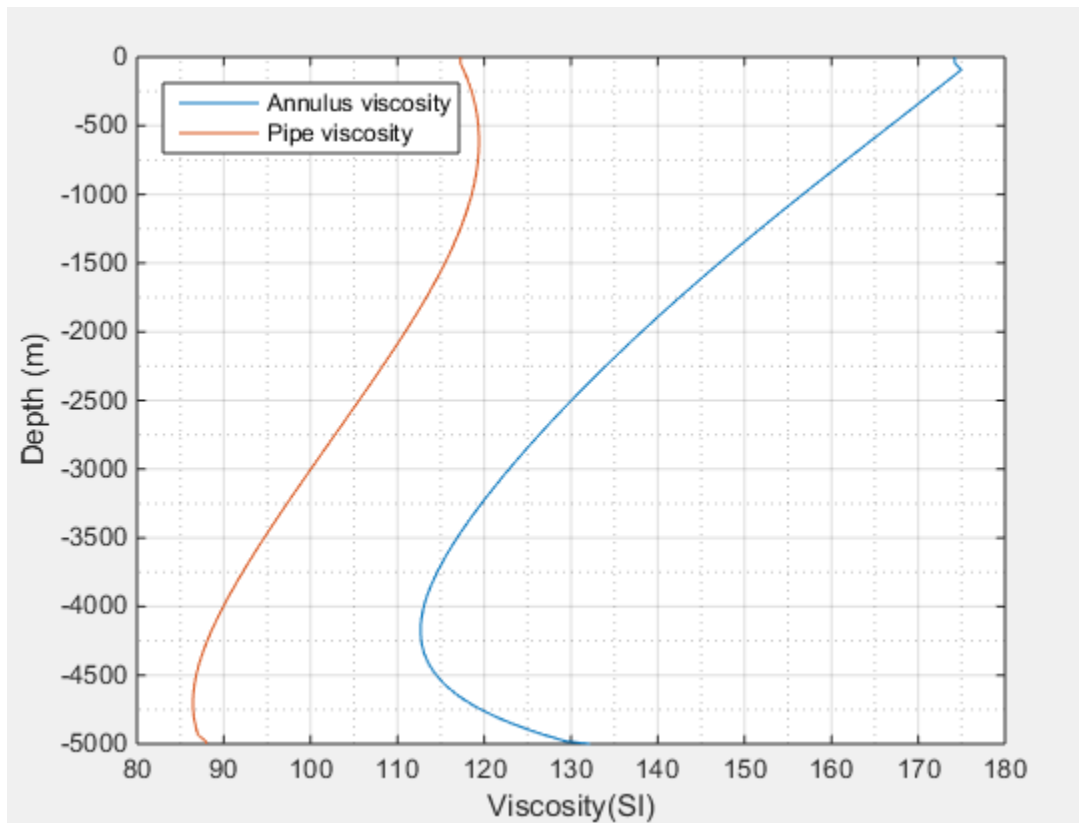
Figure 45. *Viscosity variation inside the pipe and the annulus*
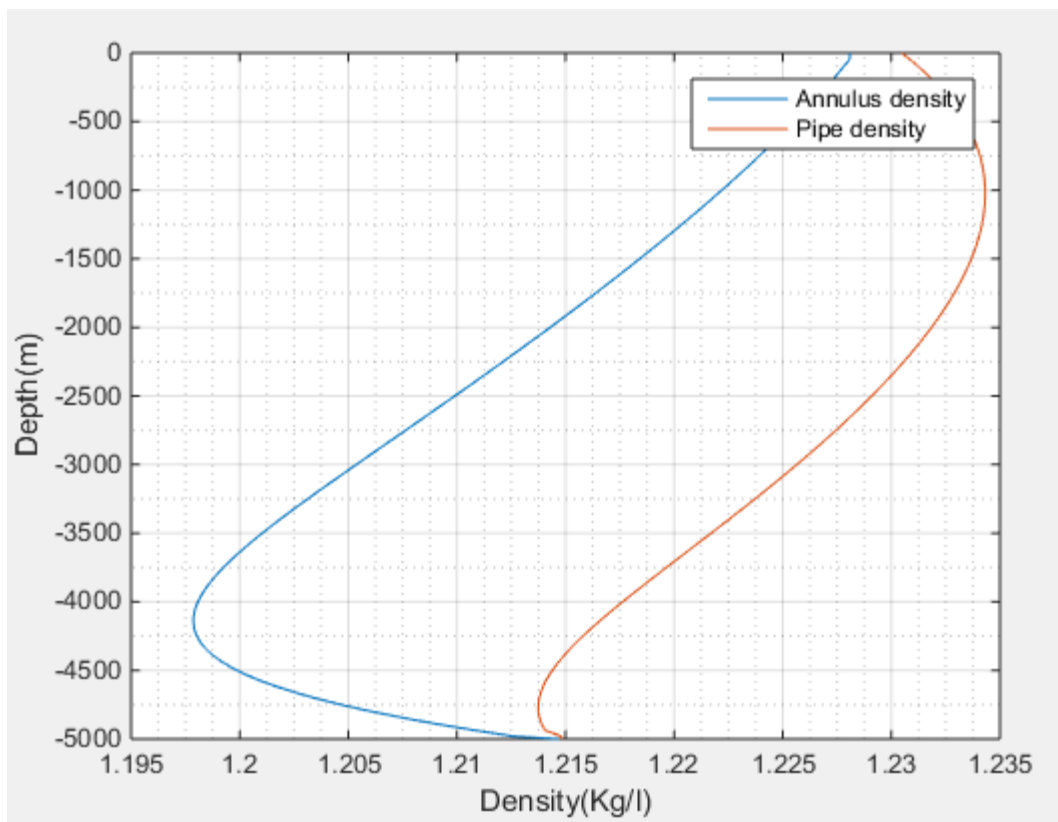
Figure 46. *Density variations inside the pipe and the annulus*

Observations

- **Fig 43** presents the temperature distribution for variables properties where the bottom-hole temperature exceeds 104°C while the outlet temperature is near 43°C.
- **Fig 44** reveals that the bottom hole temperature is near 80°C and the outlet temperature is equal to 50°C.
- Viscosity inside the annulus varies from 130 SI to 170 Si and it varies from 90SI to 115 SI inside the pipe.
- Density varies from 1215 kg/m^3 to 1230 kg/m^3. (Observations from **Fig 45** and **Fig 46**).

Explanations

From the observations made on the two figures, differences of temperature between the two cases are remarkable confirming that the effect of pressure and temperature on fluid properties cannot be neglected. **Fig 45** shows that viscosity is affected by pressure and temperature more than density. This alteration affects the temperature distribution greatly.

4.8 Effect of energy sources

The external energy sources play an important role at determining the temperature distribution inside the wellbore during transient state. For a more accurate prediction of the temperature function, taking in consideration the heat released due to: friction, pressure losses and Joule-Thompson effect is necessary.

To verify these assumptions, a comparative study between a case where the external heat sources are considered, and a second case where the effect of external energy sources are neglected is proceeded. **Fig 47** and **Fig 48** shows the results of this comparative study. **Fig 47** presents the temperature distribution where the effect of the external energy sources is considered. **Fig 48** shows the simulation results when these effects are neglected.
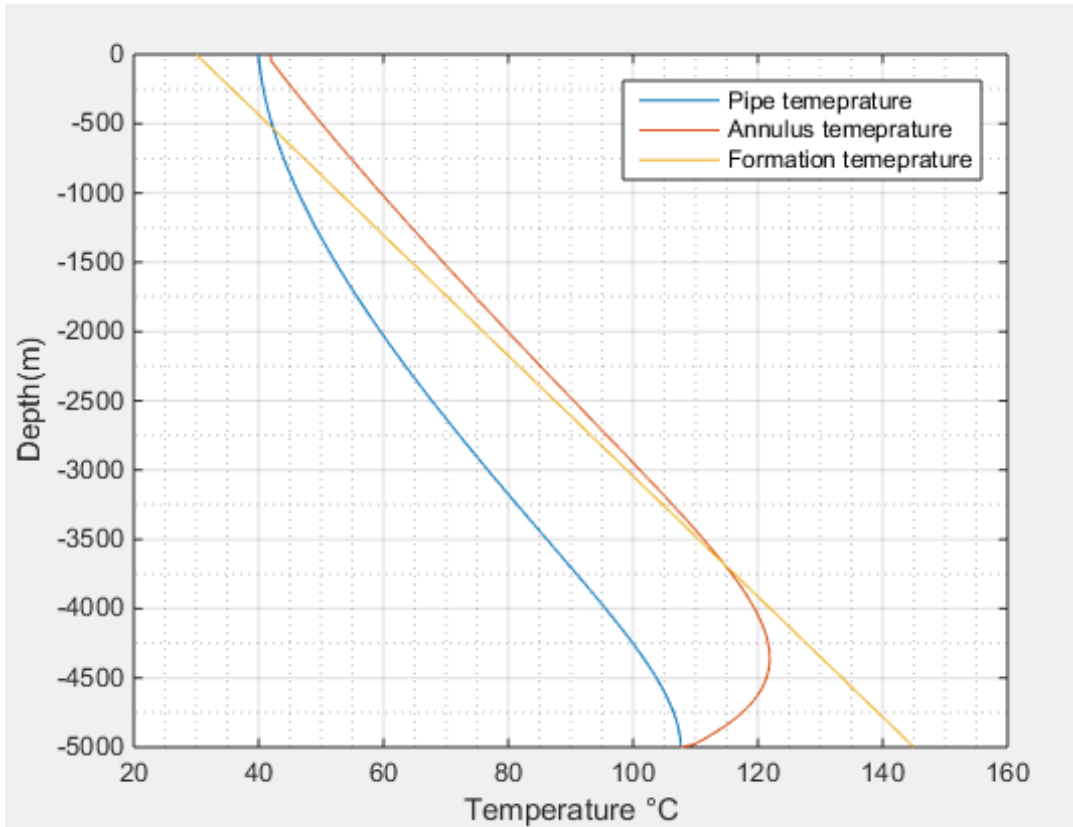
Figure 47. *Temperature distribution with external energy sources*
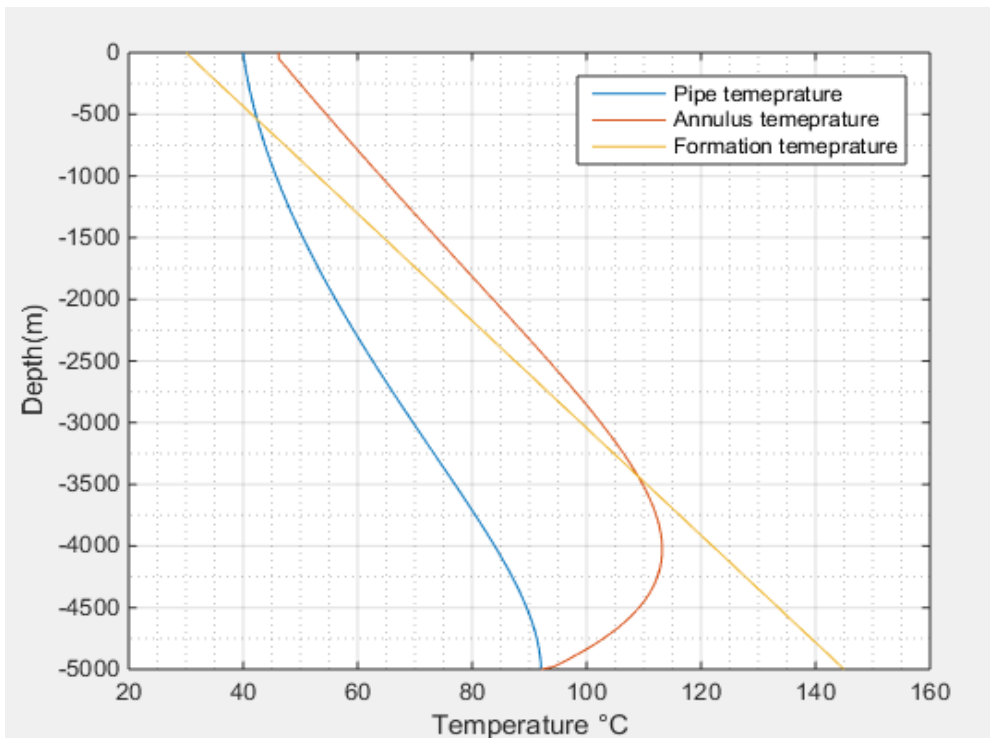
Figure 48*. Temperature distribution without external energy sources*

Observations

- Analyzing **Fig 47** shows that temperature inside the pipe and the annulus tends to increase at each depth with a temperature approaching 107 °C at the bottom and a higher outlet temperature reaching a value of 43°C.

- **Fig 48** reveals that the temperature of the fluid inside both the pipe and the annulus tend to decrease compared to the temperature when the external heat sources are taken into account. It takes a value of 92°C at the bottom hole and an outlet temperature of 47°C.

Explanation

This observations lead to the conclusion that heat coming from external energy sources cannot be neglected and have a great impact on the fluid and that by increasing its temperature. For a same node, the difference of temperature between the two conditions(with and without external energy sources effects) increases the more the node is near the bottom-hole, since the results shows a difference of 15°C at the bottom-hole and a difference of 2°C at the outlet.

4.9 Circulation time

Circulation time is the time from the beginning of the circulation (the fluid is on its initial conditions and takes the values of formation' temperature), until the flow of the fluid stops. Depending on this time interval, fluid exposed to different heat sources undergoes temperature alterations. A range of time during which fluid's temperature changes, before the fluid enters a steady state (where the temperature remains constant with time), will be determined in the simulations. This range depends on different parameters (Increasing the flow rate, for instance, decreases the time the fluid needs to reach the steady state).

Fig 49, **Fig 50**, **Fig 51** and **Fig 52** shows the simulation results of the studied fluid in 4 different times respectively: 10 min, 30 mi, 2 hours and the steady state finally for an infinite time.
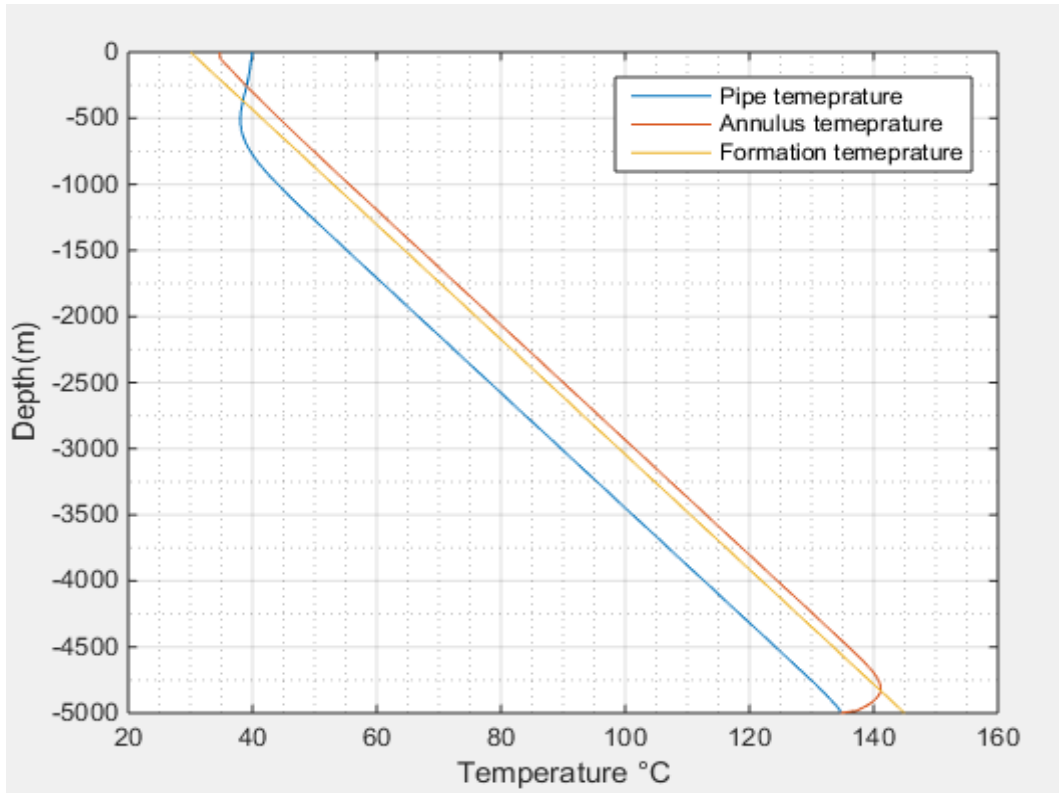
Figure 49. *Temperature distribution for a circulation time of 10min*
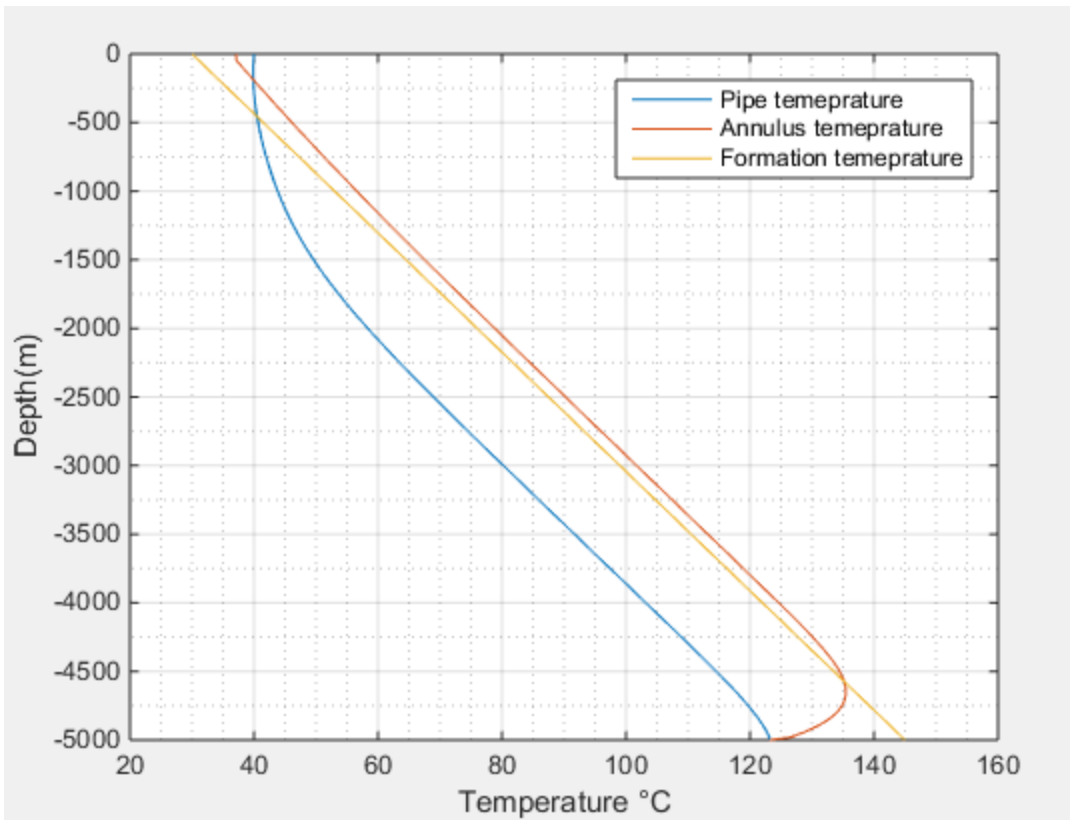
Figure 50. *Temperature distribution for a circulation time of 30 min*
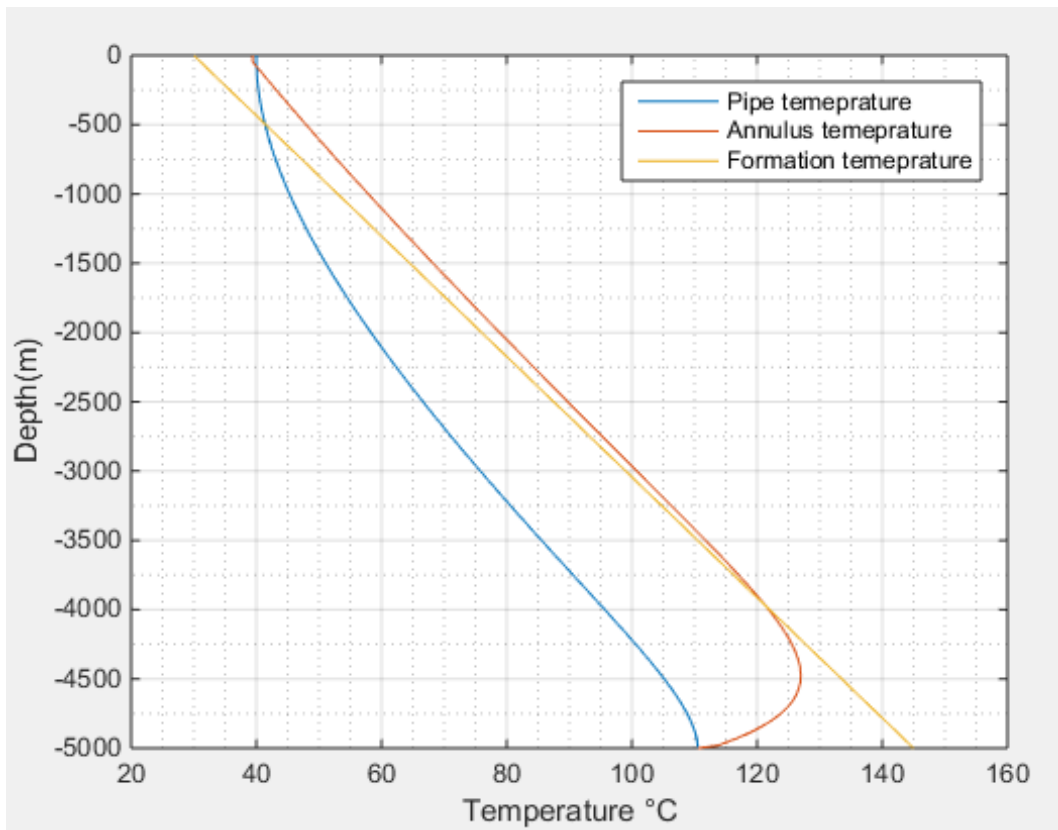
Figure 51*. Temperature distribution for a circulation time of 2 hours*
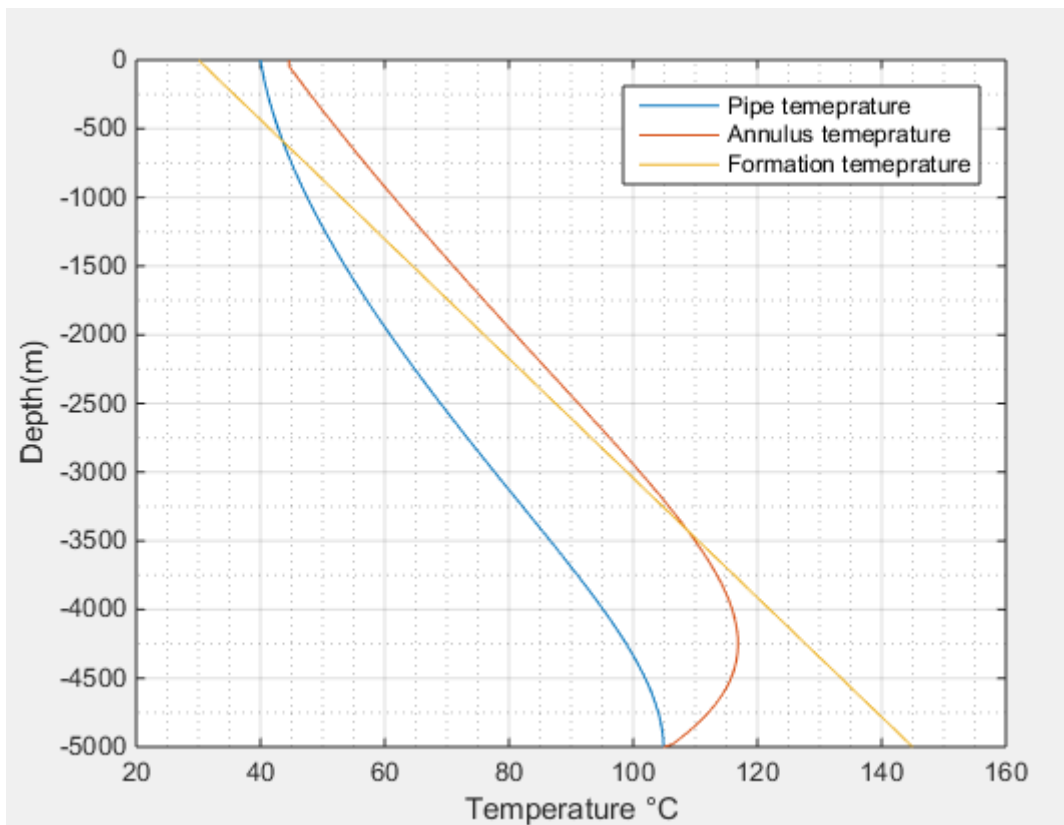
Figure 52*. Temperature distribution for a circulation time of 10 hours*

Observation

Fig 49, 50, 51 and **52** show that the temperature of the fluid decreases with time, shifting from its initial conditions to the steady state where temperature will be time' independent.

General Conclusion

General conclusion

In this thesis, the chief aim was to give the reader an inclusive and a realistic model for the drilling fluid' temperature during a transient state, a goal achieved successfully by using a model which gives realistic and acceptable results for the temperature distribution.

The difference between these work and other similar ones is the details contained, that you cannot find in most available documents, which only give the head start equations and don't deepen enough into details.

The different equations governing the fluid' temperature inside the pipe and the annulus are given after defining all the different terms composing these equations. The explicit finite element method is than used to resolve the differential equations obtained using the first law of thermodynamics. The matrixial system is solved using a MATLAB code where some of its parts were presented in order to help the reader implement the different MATAB commands easily.

The simulations of the last chapter are presented to investigate which parameters affect the temperature the most. This can help engineers manipulate these parameters in order to control the temperature distribution. In these simulations, we found that different parameters affect the temperature distribution like heat capacity, density and many other parameters. Changing these parameters allows us to control the temperature.

References

[1] Kevin Graham Harding. Heat transfer introduction. 2018.

[2] T.R. Marshall and O.H. Lie, * Baker Jardine & Assocs. Inc. A Thermal Transient Model of Circulating Wells, SPE 24290. 1992.

[3] Dan Sui, Vebjorn Haraldstad Langaker. Downhole Temperature Modeling for Non-Newtonian Fluids in ERD Wells. Petroleum Engineering Department, University of Stavanger, Norway, 4036. 2018

[4] Mostafa Abdel hafiz, Luiz A Hegele Jr. Temperature Modeling for Wellbore Circulation and Shut-in with Application in Vertical Geothermal Wells. Journal of Petroleum Science and Engineering · March 2021.

[5] E. E. Santoyo *, A. Garcia, G. Espinosa, S. Santoyo-Gutirrez, E. Gonzalez-Partida. Convective heat-transfer coefficients of non-Newtonian geothermal drilling fluids. National Autonomous University of Mexico, Temixco, Mor. 62580, Mexico

[6] B. Corre, R. Eymard, and A. Guenot, Numerical computation of temperature distribution in a wellbore
while drilling. SPE 13208. September 1984.

[7] A. R. Hasan, C, S, Kabir. A Fluid Circulating Temperature Model for Workover Operations. 1996.

[8] Bergman, Theodore L, Frank P Incropera, David P DeWitt, and Adrienne S Lavine. Fundamentals of heat and mass transfer, 2011.

[9] F.J. McQuillan, J.R. Culham and M.M. Yovanovich, Properties of dry air at one atmosphere.

[10] O.O. Harris, S.O. Osisanya. Evaluation of Equivalent Circulating Density of Drilling Fluids Under High-Pressure/ High-Temperature Conditions. SPE 97018

[11] Wikipedia. Mud weight.

[12] Sofiane KOUZRITE, Numerical modeling of a fluid temperature during drilling operations, PFE project,2020.

[13] Crank, J. The mathematics of diffusion. 2nd Edition, Oxford, 1975.

[14] Randall J. LeVeque. Finite Difference Methods for Differential Equations. University of Washington Version of September, 2005.

[15] Xin Chang 1,2, Jun Zhou 1,2,*, Yintong Guo 1,2, Shiming He 3,*, Lei Wang 1,2, Yulin Chen 4, Ming Tang 3 and Rui Jian. Heat Transfer Behaviors in Horizontal Wells Considering the Effects of Drill Pipe Rotation, and Hydraulic and Mechanical Frictions during Drilling Procedures

[16] Ebrahim Hajidavalloo, Alireza Daneh-Dezfuli, Effect of temperature variation on the accurate prediction of bottom-hole pressure in well drilling, July 2020.

[17] Zheng Zhang, Youming Xiong, Hui Pu, Zheng Sun. Effect of the variations of thermophysical properties of drilling fluids with temperature on wellbore temperature calculation during drilling.2020

[18] GEFEI LIU,Pegasus Vertex, Inc., Houston, TX, United States, APPLIED WELL CEMENTING ENGINEERING.

[19] Mostafa M. Abdelhafiz a,b, Luiz A. Hegele Jr a,c,∗, Joachim F. Oppelt a,Numerical transient and steady state analytical modeling of the wellbore temperature during drilling fluid circulation.

[18] https://www.rigzone.com/training/insight.asp?insight_id=295&c_id= , Figure 1.

[19] https://www.researchgate.net/figure/Schematic-layout-of-petroleum-drilling-rig-with-top-drive-and-draw-works-drives-for_fig2_339285464 , Figure 2.

[20] https://data.epo.org/publication-server/document?iDocId=272596&iFormat= , Figure 3.